

Rapid evaluation of notch stress intensity factors using the peak stress method with 3D tetrahedral finite element models: Comparison of commercial codes

Giovanni Meneghetti¹  | Alberto Campagnolo¹  | Alberto Visentin¹ 
 Massimiliano Avalle² | Matteo Benedetti³  | Andrea Bighelli³ |
 Davide Castagnetti⁴  | Andrea Chiocca⁵  | Luca Collini⁶  |
 Massimiliano De Agostinis⁷ | Alessandro De Luca⁸ | Eugenio Dragoni⁴ |
 Stefano Fini⁷ | Vigilio Fontanari³ | Francesco Frendo⁵  | Alessandro Greco⁸  |
 Giuseppe Marannano⁹ | Fabrizio Moroni⁶ | Antonio Pantano⁹ |
 Alessandro Pirondi⁶ | Alessandro Rebora² | Alessandro Scattina¹⁰  |
 Raffaele Sepe¹¹  | Andrea Spaggiari⁴ | Bernardo Zuccarello⁹

¹Department of Industrial Engineering,
 University of Padova, Padova, Italy

²Department of Mechanical, Energy,
 Management and Transportation
 Engineering, University of Genova,
 Genova, Italy

³Department of Industrial Engineering,
 University of Trento, Trento, Italy

⁴Department of Sciences and Methods for
 Engineering, University of Modena and
 Reggio Emilia, Reggio Emilia, Italy

⁵Department of Civil and Industrial
 Engineering, University of Pisa, Pisa, Italy

⁶Department of Engineering and
 Architecture, University of Parma, Parma,
 Italy

⁷Department of Industrial Engineering,
 University of Bologna, Bologna, Italy

⁸Department of Engineering, University of
 Campania "Luigi Vanvitelli", Aversa, Italy

⁹Dipartimento di Ingegneria, Università di
 Palermo, Palermo, Italy

¹⁰Department of Mechanical and
 Aerospace Engineering, Politecnico di
 Torino, Torino, Italy

¹¹Department of Industrial Engineering,
 University of Salerno, Fisciano, Italy

Abstract

The peak stress method (PSM) allows a rapid application of the notch stress intensity factor (NSIF) approach to the fatigue life assessment of welded structures, by employing the linear elastic peak stresses evaluated by FE analyses with coarse meshes. Because of the widespread adoption of 3D modeling of large and complex structures in the industry, the PSM has recently been boosted by including four-node and ten-node tetrahedral elements of Ansys FE software, which allows to discretize complex geometries. In this paper, a Round Robin among eleven Italian Universities has been performed to calibrate the PSM with seven different commercial FE software packages. Several 3D mode I, II and III problems have been considered to investigate the influence of (i) FE code, (ii) element type, (iii) mesh pattern, and (iv) procedure to extrapolate stresses at FE nodes. The majority of the adopted FE software packages present similar values of the PSM parameters, the main source of discrepancy being the stress extrapolation method at FE nodes.

KEY WORDS

coarse mesh, FE analysis, notch stress intensity factor (NSIF), peak stress method (PSM), tetrahedral element

Correspondence

Giovanni Meneghetti, Department of Industrial Engineering, University of Padova, Via Venezia, 1-35131 Padova, Italy.
Email: giovanni.meneghetti@unipd.it

1 | INTRODUCTION

In the context of the fatigue design of welded components, design codes and recommendations^{1,2} suggest several methods, namely the nominal stress,^{3,4} the structural hot-spot stress,^{3–7} the notch stress^{3,4,8–17} and the Linear Elastic Fracture Mechanics (LEFM)^{3,13,15,17–20} approaches. Additionally, criteria based on local parameters, such as stress, strain or strain energy, proved to be reliable for fatigue design of welded components, especially when complex welded details or load conditions are considered.^{10,21–23} Among these, the most widely adopted are based on Notch Stress Intensity Factors (NSIFs),^{24–27} averaged strain energy density (SED),^{13,26–31} critical plane concepts^{21,22,32} and the Theory of Critical Distances (TCD).^{9,22,33,34} The NSIF-based approach assumes the worst-case geometry both at the weld toe and at the weld root of the joint, which are idealized as sharp V-notches having null tip radius ($\rho = 0$) and opening angles of 135° and 0°, respectively, as highlighted in Figure 1A. The NSIFs permit to quantify the intensity of the singular, linear elastic stress fields close to a sharp V-notch tip. As an example, Figure 1B shows the mode I, II, and III local stress components acting at the weld toe of a partial-penetration tube-to-flange welded joint subjected to a combined bending and torsion loading. Williams³⁶ first derived analytically the singular, linear elastic stress field ahead of a sharp V-notch tip under mode I and II loadings. Afterwards, Qian and Hasebe³⁷ determined the singular stress distributions due to sharp V-notches subjected to mode III loading. Later on, Gross and Mendelson³⁸ defined the mode I, II and III NSIF-terms by means of Equations (1)–(3), respectively:

$$K_1 = \sqrt{2\pi} \cdot \lim_{r \rightarrow 0} [(\sigma_{\theta\theta})_{\theta=0} \cdot r^{1-\lambda_1}] \quad (1)$$

$$K_2 = \sqrt{2\pi} \cdot \lim_{r \rightarrow 0} [(\tau_{r\theta})_{\theta=0} \cdot r^{1-\lambda_2}] \quad (2)$$

$$K_3 = \sqrt{2\pi} \cdot \lim_{r \rightarrow 0} [(\tau_{\theta z})_{\theta=0} \cdot r^{1-\lambda_3}] \quad (3)$$

In previous expressions the terms λ_1 , λ_2 , and λ_3 represent the stress singularity degrees,^{36,37} which depend on

the V-notch opening angle 2α . Values of λ_1 , λ_2 and λ_3 referring to some notch opening angles, that is, $2\alpha = 0^\circ$, 90° , 120° , and 135° , are listed in Table 1. It is worth mentioning that the mode II stresses are not singular for notch opening angles $2\alpha > 102^\circ$ as demonstrated in Refs.,^{36,39} which very often simplifies the analysis at the weld toe where $2\alpha = 135^\circ$. Finally, the stress components in Equations (1)–(3) are referred to a cylindrical reference system (see Figure 1B) centered at the V-notch tip, where the z direction is tangent to the notch tip line and the θ -direction originates from the notch bisector line, r being the radial coordinate. Accordingly, σ_{00} , τ_{r0} , and τ_{0z} are calculated ahead of the notch tip ($r \rightarrow 0$) and along the notch bisector line ($\theta = 0$).

NSIF-parameters have been widely adopted in the literature to correlate the fatigue strength of arc-welded joints undergoing uniaxial^{24,40–42} or multiaxial²⁵ loading conditions. Nevertheless, it should be noted that the calculation of NSIF-terms on the basis of the results of numerical analyses shows a major drawback in engineering applications, since very refined FE meshes (finite element size on the order of 10^{-5} mm were adopted for 2D numerical analyses in previous reference²⁴) are required in order to apply Equations (1)–(3). When dealing with three-dimensional, complex and large-scale notched structures, both the solution of the FE model and the post-processing of numerical results could be even more time-consuming. To overcome this drawback, an engineering and rapid technique, the peak stress method (PSM), has been proposed to speed up the calculation of the NSIF-terms by adopting coarse FE analyses, the element size being some orders of magnitude larger than that required to apply Equations (1)–(3). The PSM takes inspiration from the contribution by Nisitani and Teranishi,⁴³ who proposed a technique to readily estimate the mode I Stress Intensity Factor (SIF) of a crack propagating from an ellipsoidal cavity. The PSM has been first justified theoretically and later on extended to allow the rapid calculation also of the NSIF relevant to sharp and open V-notches under mode I^{44,45}, the SIF of cracks under mode II⁴⁶ and, finally, the NSIF of open V-notches under mode III.⁴⁷

Practically, the PSM is a numerical tool, which takes advantage of the opening, in-plane shear and out-of-

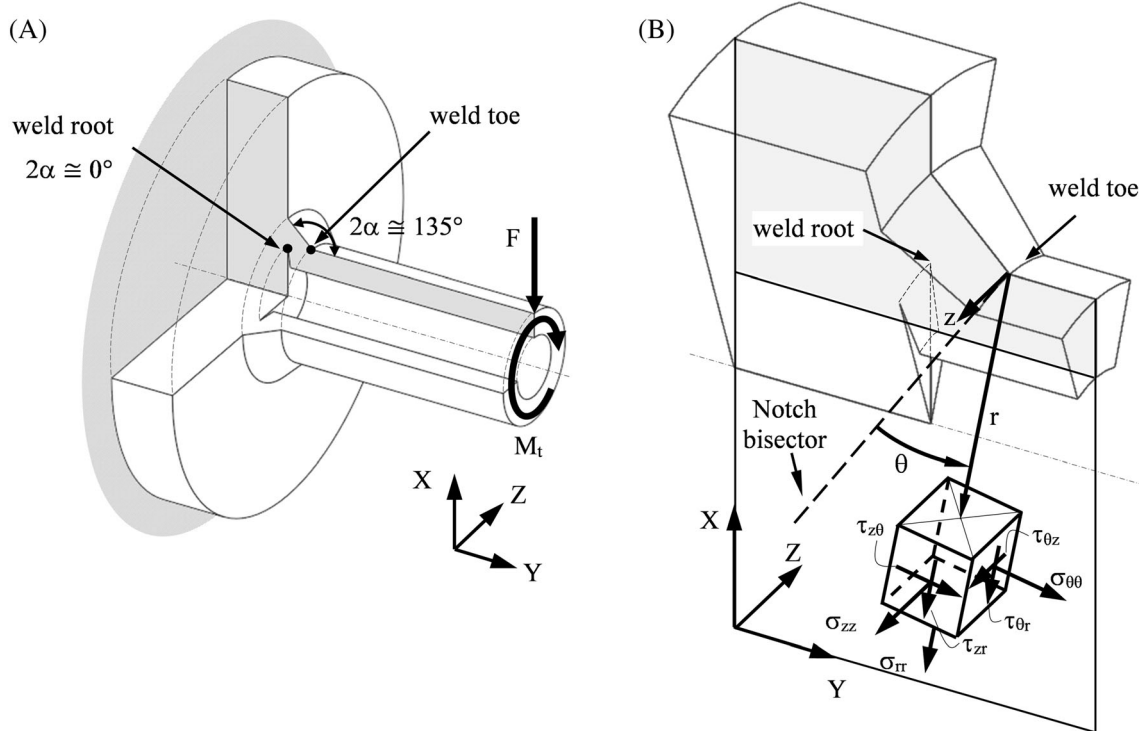


FIGURE 1 (A) Partial-penetration tube-to-flange welded joint under combined bending and torsion fatigue loading. The sharp V-notch opening angle 2α is typically 0° at the weld root and 135° at the weld toe. (B) Cylindrical reference system (r, θ, z) centered at the weld toe and singular stress components. See also previous work³⁵

TABLE 1 Parameters depending on the notch opening angle 2α

2α (°)	λ_1 ^a	λ_2 ^a	λ_3 ^b
0	0.500	0.500	0.500
90	0.545	0.909	0.667
120	0.616	—	0.750
135	0.674	—	0.800

^aValues derived from Williams.³⁶

^bValues derived from Qian and Hasebe.³⁷

plane shear peak stresses evaluated from a linear elastic FE analysis with coarse mesh (see an example in Figure 2) to rapidly estimate the NSIF-terms K_1 , K_2 , and K_3 , respectively, according to the following expressions^{44,46,47}:

$$K_1 \cong K_{FE}^* \cdot \sigma_{\theta\theta,\theta=0,peak} \cdot d^{1-\lambda_1} \quad (4)$$

$$K_2 \cong K_{FE}^{**} \cdot \tau_{r\theta,\theta=0,peak} \cdot d^{1-\lambda_2} \quad (5)$$

$$K_3 \cong K_{FE}^{***} \cdot \tau_{\theta z,\theta=0,peak} \cdot d^{1-\lambda_3} \quad (6)$$

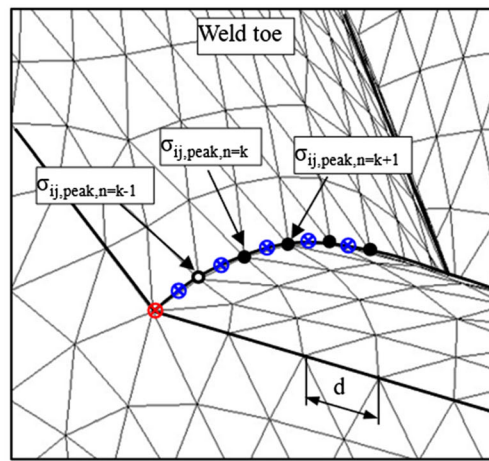
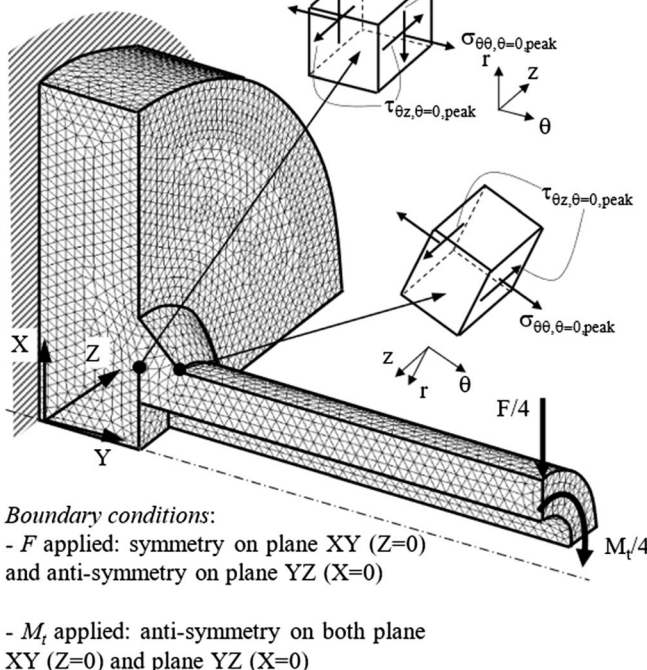
where $\sigma_{\theta\theta,\theta=0,peak}$, $\tau_{r\theta,\theta=0,peak}$ and $\tau_{\theta z,\theta=0,peak}$ are the peak stresses calculated with respect to a local cylindrical coordinate system as above, which must be centered at

the node located at the V-notch tip. The subscript “ $\theta = 0$ ” defines the direction along which peak stresses have to be calculated; as an example $\sigma_{\theta\theta,0=0,peak}$ represents the opening stress acting normal to the notch bisector, as highlighted in Figure 2. The parameter d is the average finite element size adopted by the free mesh generation algorithm available in the FE code. Finally, K_{FE}^* , K_{FE}^{**} , and K_{FE}^{***} are coefficients which must be calibrated to account for⁴⁸ (i) the element type and integration scheme; (ii) the free mesh pattern and (iii) the procedure adopted by the FE code to extrapolate the stresses at nodes.

The PSM according to Equations (4)–(6) has been calibrated in previous investigations by employing several 2D and 3D element types and commercial FE codes. First, the parameters K_{FE}^* , K_{FE}^{**} , and K_{FE}^{***} have been calibrated by using 2D, four-node plane quadrilateral elements of Ansys Mechanical APDL element library.^{44,46,47} Subsequently, a Round Robin Project was run⁴⁸ to calibrate the coefficients K_{FE}^* and K_{FE}^{**} for 2D, four-node plane quadrilateral elements available in six commercial FE packages other than Ansys Mechanical APDL, namely Abaqus, Straus7, MSC Patran/Nastran, LUSAS, HyperMesh/OptiStruct/HyperView, and HyperMesh/LS-Dyna/HyperView. A further development consisted in extending the PSM to 3D, eight-node brick elements,⁴⁵ by taking advantage of the submodeling technique of

PSM based on TETRAHEDRAL elements

Example: SOLID 187 of Ansys® element library



- node at free-surface is excluded from PSM calculations
- mid-side nodes are excluded
- node where average peak stresses cannot be defined
- node where average peak stresses can be defined

FIGURE 2 FE model to apply the PSM according to Equations (4)–(6) to a partial-penetration tube-to-flange welded joint under combined bending and torsion loading using ten-node tetrahedral elements. See also previous work³⁵ [Colour figure can be viewed at wileyonlinelibrary.com]

Ansys® FE software. More precisely, when considering a complex 3D welded structure, first, a main model having a free-mesh of ten-node tetrahedral elements is solved and then a submodel of the critical region is meshed with a regular pattern of eight-node brick elements and eventually analyzed with the PSM.

Given the ever increasing adoption of three-dimensional modeling of large-scale complex structures in the industry, the 3D PSM has recently been improved by calibrating coefficients K_{FE}^* , K_{FE}^{**} , and K_{FE}^{***} for four-node and ten-node tetrahedral elements^{49,50} of Ansys Mechanical APDL element library. These finite element types allow to easily discretize complex three-dimensional geometries and to apply the PSM directly to the free-meshed main model, making the submodel with regular mesh pattern unnecessary. Nevertheless, mesh patterns consisting of tetrahedral elements are typically irregular, in the sense that each node belonging to the notch tip line can be shared by a different number of elements and have significantly different sizes and shapes (see for example next Figure 10). As a consequence, the peak stress components could vary along the notch tip line, even in cases where the NSIF-parameters are constant. To smooth the peak stress distribution along the notch tip line, the average peak stress has been

introduced and it was defined as the moving average of peak stresses evaluated on three adjacent vertex nodes.⁴⁹ For example, the average peak stress at node $n = k$ is calculated as follows:

$$\bar{\sigma}_{ij,peak,n=k} = \frac{\sigma_{ij,peak,n=k-1} + \sigma_{ij,peak,n=k} + \sigma_{ij,peak,n=k+1}}{3} \Big|_{n=node} \quad (7)$$

Therefore, the PSM-coefficients K_{FE}^* , K_{FE}^{**} , and K_{FE}^{***} have been calibrated in previous works^{49,50} by adopting four-node and ten-node tetrahedral elements and by input the average peak stress components according to Equation (7) into Equations (4)–(6), that is, $\bar{\sigma}_{\theta\theta,\theta=0,peak}$, $\bar{\tau}_{r\theta,\theta=0,peak}$, and $\bar{\tau}_{\theta z,\theta=0,peak}$ in place of the peak stresses $\sigma_{\theta\theta,0=0,peak}$, $\tau_{r\theta,0=0,peak}$, and $\tau_{\theta z,0=0,peak}$, respectively. Furthermore, Figure 2 highlights that (i) the PSM based on tetrahedral elements cannot be applied at nodes laying on a free surface of the considered notched structure,^{49,50} since peak stress values at those nodes are affected by the distorted mesh pattern; (ii) peak stresses must be calculated only at vertex nodes of ten-node tetrahedral elements; that is, peak stresses existing at mid-side nodes must be neglected. Previous item (i) implies that

the nearest node from a free surface where the peak stress can be evaluated according to Equation (7) is the third vertex node of the tetrahedral element mesh. If the fatigue critical location is at the free surface, the PSM prevent the FE analyst from evaluating the equivalent peak stress exactly at the crack initiation point. As an example, in the case of the tube-to-flange full-penetration joint tested under bending loading by Sonsino (see previous works^{21,51} and Figure 2), a 7% difference was found between the equivalent peak stress evaluated at the point of crack initiation (by using one half of the model, not reported in Figure 2) and at the third vertex node (by using one fourth of the model according to Figure 2), which was considered acceptable. Otherwise, the coarse FE mesh according to the PSM must be locally refined to place the third vertex node closer to the critical location.

The comparison between Equations (4)–(6) and previous Equations (1)–(3) shows that the PSM has a further advantage in addition to the coarse FE mesh: only a single linear-elastic peak stress evaluated at the singularity location is necessary to estimate each NSIF-term, instead of a number of *stress* versus *distance* results, which require a post-processing analysis. Other methods^{52–56} are available in the literature to rapidly estimate the NSIF-terms using coarse meshes. Lazzarin et al.⁵³ suggested to take advantage of the averaged SED calculated by adopting coarse meshes inside a structural volume of radius R_0 . The need for the geometrical modeling of the structural volume has been removed in very recent contributions by Foti et al.,⁵⁶ Campagnolo et al.,⁵⁷ and Zappalorto et al.^{54,55} in case of 2D problems. It is worth noting that the values of K_{FE}^* , K_{FE}^{**} , and K_{FE}^{***} calibrated under pure modes of loading using 2D four-node plane elements, 3D eight-node brick elements, four-node as well as ten-node tetrahedral elements of Ansys Mechanical APDL element library have been successfully checked also against mixed mode problems.^{58–61}

Incidentally, thanks to Equations (4)–(6), any NSIF-based approach for the structural strength assessment of notched structures can in principle be reformulated on the basis of the PSM. Recently, the PSM has been applied in combination with the approach based on the averaged SED to assess the fatigue strength of welded joints under axial,^{46,62} torsion⁴⁷ and multiaxial^{51,63} loading conditions. More precisely, the PSM based on tetrahedral elements has been adopted for the fatigue strength assessment of large-scale and geometrically complex welded structures taken from industrial case studies, for example a roundabout-type carousel, a scotch-yoke valve actuator, a suspension for cableway vehicles and a sluice gate. The results have been reviewed in Ref.,⁶⁴ where a very good agreement has been observed between the PSM-based results and those obtained by different approaches in

terms of estimated NSIF-parameters or averaged SED. For additional details, the reader is referred to the recent state-of-the-art reviews focused on NSIF,⁶⁵ averaged SED^{66,67} and PSM³⁵ approaches.

To broaden the possibility of using the PSM with 3D tetrahedral finite element models, it is of paramount importance to calibrate the parameters K_{FE}^* , K_{FE}^{**} , and K_{FE}^{***} for commercial FE packages other than Ansys. Therefore, following the track of the previous Round Robin⁴⁸ focused on the 2D PSM, the present investigation presents the results of a new Round Robin which has been performed to determine K_{FE}^* , K_{FE}^{**} , and K_{FE}^{***} for 3D tetrahedral finite element models. To the best of authors' knowledge, the 3D PSM based on tetrahedral elements of FE codes other than Ansys has been adopted only in a recent paper⁶⁸, where the NSIFs resulting from welding residual stresses have been rapidly estimated in steel butt-welded joints using Sysweld.

The work plan of the present Round Robin consisted in applying the PSM to several 3D V-notch problems under pure mode I, pure mode II and pure mode III loadings by adopting four-node or ten-node tetrahedral elements available in different FE software packages. After having evaluated the peak stresses from the FE models and the average peak stresses according to Equation (7), the non-dimensional parameters K_{FE}^* , K_{FE}^{**} , and K_{FE}^{***} have been calculated using Equations (4)–(6), but now rearranged in the following way:

$$K_{FE}^* \cong \frac{K_1}{\bar{\sigma}_{\theta\theta,\theta=0,peak} \cdot d^{1-\lambda_1}} \quad (8)$$

$$K_{FE}^{**} \cong \frac{K_2}{\bar{\tau}_{r\theta,\theta=0,peak} \cdot d^{1-\lambda_2}} \quad (9)$$

$$K_{FE}^{***} \cong \frac{K_3}{\bar{\tau}_{\theta z,\theta=0,peak} \cdot d^{1-\lambda_3}} \quad (10)$$

For each numerical software package, the calibration has been carried out by keeping fixed the following analysis conditions: (i) element type and integration scheme, (ii) free mesh pattern, and (iii) procedure to extrapolate stresses at nodes.

2 | CALIBRATING THE PSM WITH 3D TETRAHEDRAL ELEMENTS OF ANSYS® MECHANICAL APDL FE CODE

The PSM parameters K_{FE}^* , K_{FE}^{**} , and K_{FE}^{***} appearing in Equations (4)–(6) have been calibrated using tetrahedral

elements of Ansys Mechanical APDL in a previous paper,⁵⁰ which the reader is referred to. The obtained values are recalled in next Table 4, as a function of the loading mode, the element type and the notch opening angle, while the conditions of applicability are summarized in the following:

- the following tetrahedral elements of Ansys Mechanical APDL element library have been calibrated:
 - three-dimensional, four-node, linear tetrahedral elements (SOLID 285);
 - three-dimensional, ten-node, quadratic tetrahedral elements (SOLID 187);
- Equations (4) and (6) can be adopted to analyze sharp V-notches under mode I and III, respectively, having an opening angle $0^\circ \leq 2\alpha \leq 135^\circ$. On the other hand, Equation (5) can be applied to analyze the crack problem ($2\alpha = 0^\circ$) under mode II loading, while in a recent paper³⁵ it has been extended to treat also the case $2\alpha = 90^\circ$, which is the typical case of a weld root with a gap.
- the average size d of the tetrahedral elements defining the free mesh pattern can be chosen within the range of applicability reported in Table 4 in terms of minimum mesh density ratio a/d , adopted element type and notch opening angle. a represents the characteristic size of the considered sharp notch, e.g. a is the notch depth in Figure 3C; more precisely, a is the minimum between the V-notch depth and the ligament size (indicated as h in Figure 3). In the great majority of the notch problems considered in the present study, the characteristic size a corresponded to the notch depth since $a < h$; however, few exceptions exist in Table 3 for which $a > h$; however, to simplify the presentation of the results, a has been always adopted to identify the notch depth also in these cases.
- To apply the 3D PSM with Ansys Mechanical APDL FE code, the “Full graphics” option must be activated before evaluating the peak stresses in the post-processing environment. Ansys Mechanical APDL FE code adopts the “Power graphics” as the default option since it offers faster plotting than the “Full graphics” option. However, “Power graphics” option employs only elements and nodes lying in the exterior surface of the model to compute the results (both printed and plotted), while “Full graphics” option employs all elements and nodes (both in the interior of the model and in the surface). Therefore, the default “Power graphics” option is less accurate and must be avoided when applying the PSM.

3 | FE CODES AND PARTICIPANTS INVOLVED IN THE ROUND ROBIN

Table 2 summarizes the seven FE software packages and the eleven participants involved in the Round Robin. It is worth noting that LS-Dyna and Optistruct have been employed as solvers, while Hypermesh and Hyperview have been adopted as pre-processor and post-processor environments, respectively.

4 | GEOMETRIES, MATERIAL AND FE MESH PATTERNS

Three-dimensional mode I, II and III notch problems have been analyzed by adopting different FE codes. The considered geometries include cracks as well as sharp V-notches and not necessarily represent welded components, due to the general validity of expressions 4–6 to be calibrated. On one hand, geometries, material parameters, element types, constraint and loading conditions have been obviously kept the same in all FE software. On the other hand, as far as possible, specific settings relevant to element formulations, mesh generation algorithms and procedures to extrapolate and to average stress components at FE nodes have been set to *default options* in each FE code. In the Discussion section, to investigate the reasons for the different obtained results, additional FE analyses of the following types have been performed: (i) a FE software has been adopted enforcing the default criterion regarding the stress extrapolation at nodes of another FE code; (ii) the mesh pattern generated by a given FE code has been imported into another code in order to compare the results keeping the same FE mesh pattern. All details relevant to the FE analyses carried out and the post-processing of the results are reported in the following. As a general setting for all analyses, linear elastic, static structural analyses have been performed and a structural steel having Young's modulus $E = 206,000$ MPa and Poisson's ratio $\nu = 0.3$ has been adopted.

4.1 | 3D problems (plane strain), mode I loading, $2\alpha = 0^\circ, 90^\circ, 120^\circ, 135^\circ$

A number of 3D notch problems under pure mode I loading as sketched in Figure 3A–D have been analyzed, all geometries being the same treated in the original calibration of the PSM based on tetrahedral elements carried out using Ansys Mechanical APDL code.⁵⁰ More in detail,

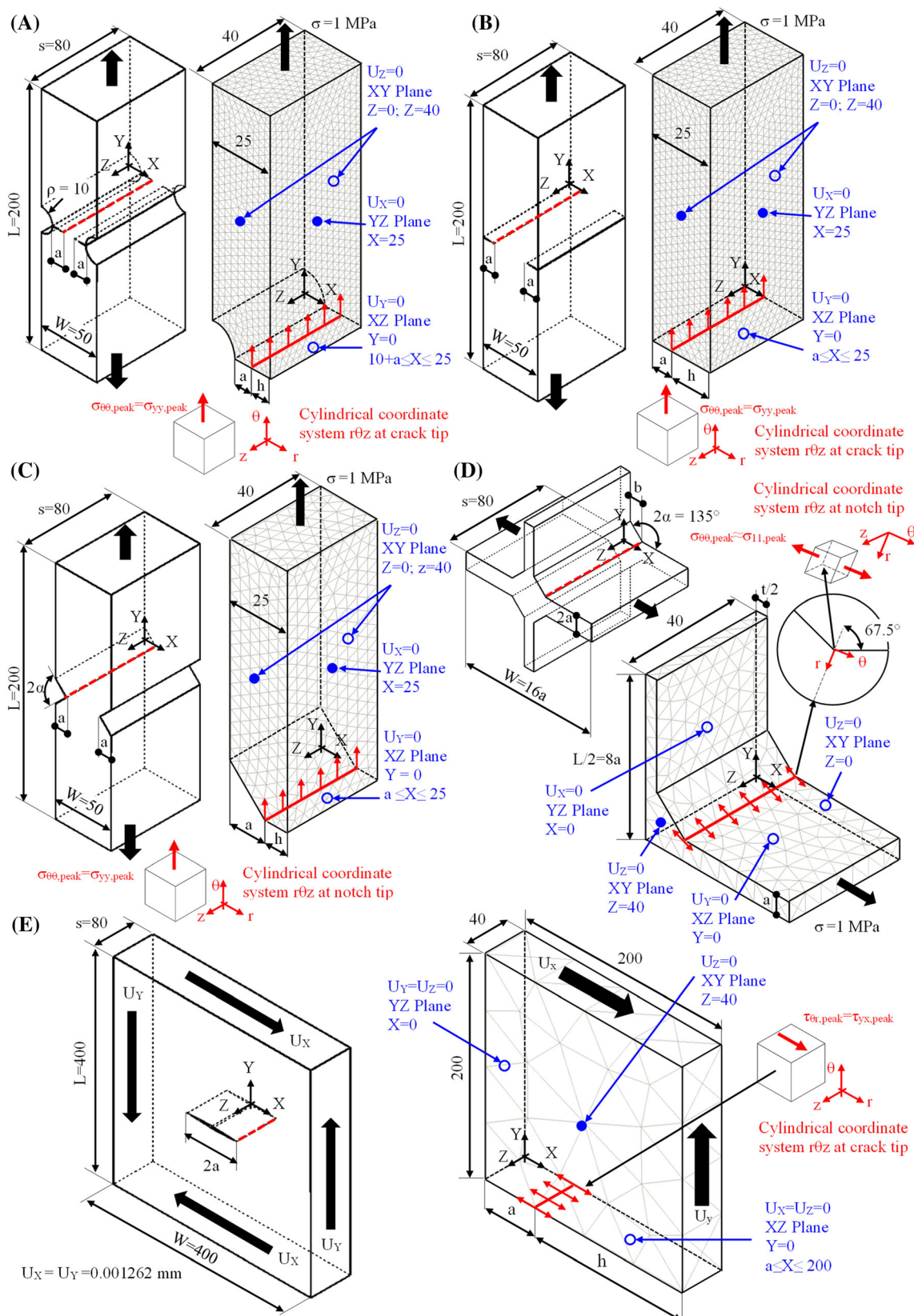


FIGURE 3 Geometries of 3D problems under mode I (A–D), mode II (E) and mode III (F–H) loadings analyzed according to the PSM. FE mesh patterns of tetrahedral elements, generated by using Ansys® mechanical APDL, and boundary conditions applied to the FE models. Dimensions are in [mm]

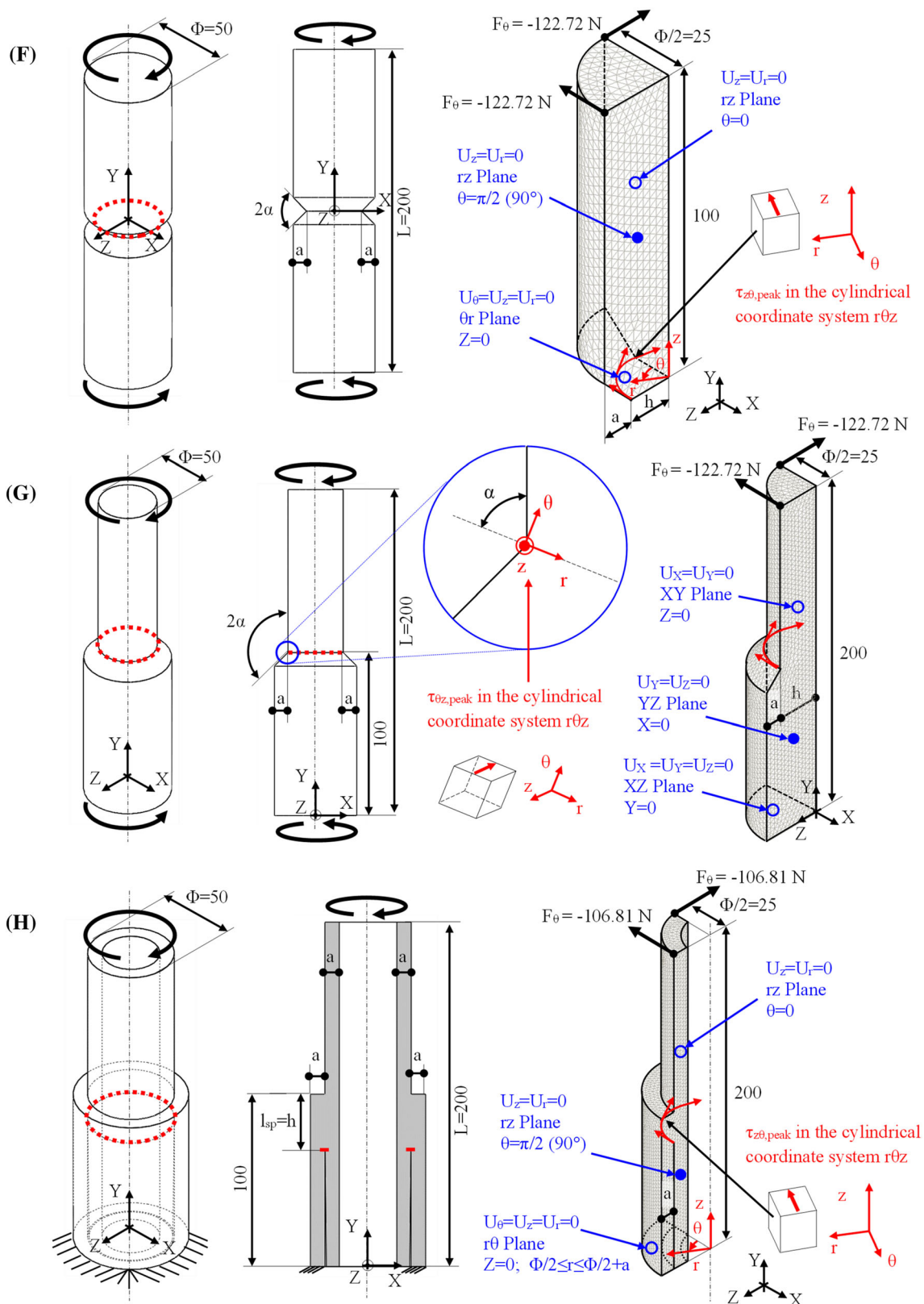


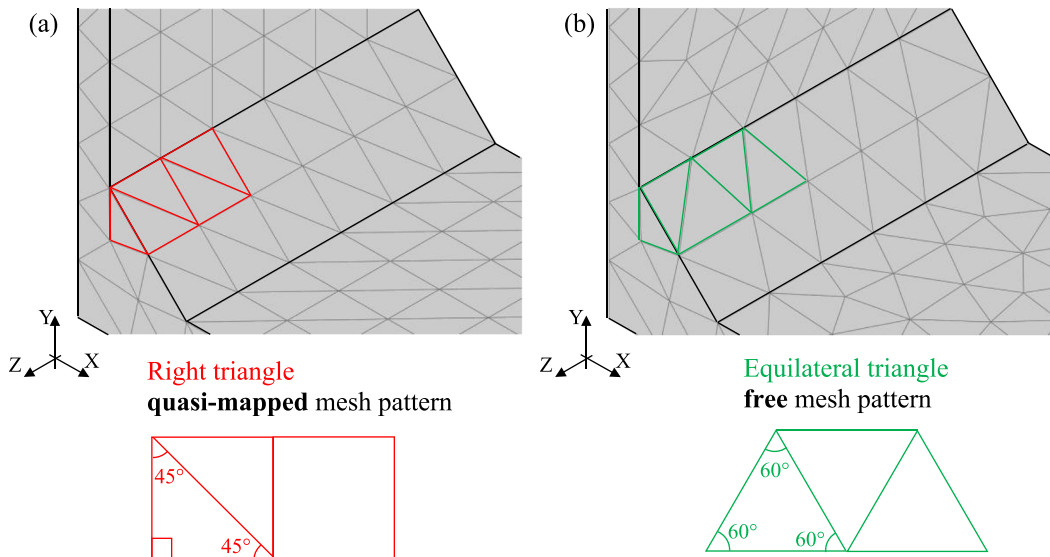
FIGURE 3 (Continued)

TABLE 2 FE codes, list of participants and information on the adopted element types and related meshing options

Software	UNI	Version	TETRA 4		TETRA 10		Meshing options	
			Element type	Gauss points	Element type	Gauss points	Mesh pattern	Other
Ansys® Mechanical APDL	UniBO	17.1	SOLID285	4	SOLID187	4	Free	n.a.
	UniGE	19 R2						
	UniPA	18.1						
	UniPD	2019 R1						
	UniPI	2019 R1						
Ansys® Mechanical^a	UniTN	17.2–18.1						
	UniPD	2020 R2	SOLID185	1	SOLID187	4	Free	n.a.
	UniSA	6.14–1	C3D4	1	C3D10	4	Free	Equi triangle
	UniCampania							
	UniPR	2019					Free	Equi triangle
Lusas®	UniMoRe	V17 (edu)	TH4	1	TH10	4	Free	n.a.
Dassault Systèmes® Solidworks	UniMoRe	2018	Draft	1	High	4	Standard (quasi-mapped)	(a) Right triangle
	UniMoRe & UniPD	2020					Blend (free)	(b) Equi triangle
Altair® Hypermesh/ LS-Dyna/Hyperview	PoliTO	2019 ^(a) R9 ^(b)	EQ-10	1	EQ-17	4	Free	n.a.
Altair® Hypermesh/ Optistruct/ Hyperview	UniGe	2019	EQ-10	1	EQ-17	4	Free	n.a.

Note: (a) Altair® Hyperworks 2019 (Hypermesh/Hyperview) version; (b) LS-Dyna R9 version (2017). n.a. = not applicable.

^aavailable within Ansys Workbench environment.



the following case studies have been considered: a crack ($2\alpha = 0^\circ$) at the tip of a U-notch (Figure 3A); a plate with lateral cracks ($2\alpha = 0^\circ$) (Figure 3B); a plate with lateral sharp V-notches ($2\alpha = 90^\circ, 120^\circ, 135^\circ$) (Figure 3C) and

the weld toe ($2\alpha = 135^\circ$) of a full-penetration cruciform welded joint (Figure 3D).

Three-dimensional analyses have been performed by adopting a mesh pattern of four-node or ten-node

tetrahedral elements, see the examples in Figure 3A–D, which refer to Ansys Mechanical APDL code. The free mesh generation algorithm available in each FE code has been executed, after having set the desired FE size d . The mesh density ratio a/d has been varied in the range between 1 and 13, by considering several values of notch/crack size a and element size d , as summarized in Table 3. One eighth of each geometry has been modeled by exploiting the triple symmetry condition; plane strain conditions have been simulated by constraining the out-of-plane displacement U_z according to Figure 3A–D, resulting in $\varepsilon_z = 0$. A pure mode I axial load has been applied to each FE model by means of a nominal gross-section tensile stress equal to 1 MPa.

After solution of the FE analyses, the opening peak stress $\sigma_{00,0=0,\text{peak}}$ has been evaluated in the post-processing environment of each FE code at vertex nodes belonging to the crack or V-notch tip lines (see Figure 3A–D). In all considered FE codes, stress averaging at FE nodes has been activated, so that only a single value of $\sigma_{00,0=0,\text{peak}}$ has been obtained per node, that is, the average of the nodal stresses from all elements sharing the node. To do this, the *default options* of each FE software have been employed, as it will be discussed in the next sections. After that, Equation (7) has been applied to calculate the average peak stress $\bar{\sigma}_{00,0=0,\text{peak}}$ at each vertex node.

The exact values of the NSIF K_1 , to be employed in Equation (8), have been computed by adopting Ansys Mechanical APDL code and by applying Equation (1) to the stress-distance results obtained from two-dimensional FE analyses under plane strain conditions. Very refined FE meshes of eight-node, quadratic quadrilateral elements (PLANE 183 of Ansys® element library), having size of the order of 10^{-5} mm close to the notch tip, have been employed.

4.2 | 3D problems (plane strain), mode II loading, $2\alpha = 0^\circ$

A crack ($2\alpha = 0^\circ$) centered in a plate (Figure 3E) has been analyzed under pure mode II loading conditions, the geometry being taken from the original calibration of the PSM based on tetrahedral elements performed with Ansys Mechanical APDL code.⁵⁰

Three-dimensional analyses have been carried out by using a free FE mesh of four-node or ten-node tetrahedral elements, see the example of Figure 3E, which refers to Ansys Mechanical APDL code. A mesh density ratio a/d in the range from 1 to 25 has been adopted, as shown in Table 3. Only one eighth of the cracked plate has been modeled taking advantage of the double anti-symmetry condition on planes YZ and XZ and of the symmetry

condition on plane XY (see Figure 3E). Pure mode II shear loading has been applied to each FE model by means of displacements $U_x = U_y = 1.262 \cdot 10^{-3}$ mm at the plate free lateral surfaces, which correspond to a nominal gross-section shear stress equal to 1 MPa in the corresponding crack-free geometry.

After solution, the in-plane shear peak stress $\tau_{r0,0=0,\text{peak}}$ has been evaluated at vertex nodes belonging to the crack tip line (Figure 3E), stress averaging at FE nodes being activated as explained above when dealing with mode I problems. Eventually, Equation (7) has been employed to calculate the average peak stress $\bar{\tau}_{r0,0=0,\text{peak}}$ at each vertex node.

Again, the exact values of the SIF K_2 , to be employed in Equation (9), have been calculated by adopting Ansys Mechanical APDL code and by applying Equation (2) to the stress-distance results derived from two-dimensional FE analyses with very refined FE meshes of eight-node, quadratic quadrilateral elements (PLANE 183 of Ansys® element library).

4.3 | 3D problems, mode III loading, $2\alpha = 0^\circ, 90^\circ, 120^\circ, 135^\circ$

Different 3D notch problems subjected to pure mode III loading as sketched in Figure 3F–H have been analyzed. All geometries are the same considered in the original calibration of the PSM based on tetrahedral elements performed using Ansys Mechanical APDL code⁵⁰. The following case studies have been treated: a circumferential crack ($2\alpha = 0^\circ$) or sharp V-notch ($2\alpha = 90^\circ, 120^\circ, 135^\circ$) in a cylindrical bar (Figure 3F); a sharp V-notch ($2\alpha = 90^\circ, 120^\circ, 135^\circ$) at a shaft shoulder (Figure 3F) and the weld root ($2\alpha = 0^\circ$) in a geometry that recalls that of a tube-to-tube welded joint (Figure 3H).

Three-dimensional analyses have been performed by employing a free mesh pattern of either four-node or ten-node tetrahedral elements, see the examples in Figure 3F–H, referred to Ansys Mechanical APDL code. The mesh density ratio a/d has been varied in the range between 1 and 10, as summarized in Table 3. A 90° segment of each cylindrical geometry has been modeled taking advantage of the double anti-symmetry condition on planes YZ and XY. Moreover, the anti-symmetry on plane XZ as well has been also employed for the geometry of Figure 3F; conversely, dealing with geometries of Figure 3G,H, the free face on plane XZ has been fully constrained. Finally, two tangential forces F_0 have been applied at single nodes having X-Z coordinates $(-\Phi/2, 0)$ and $(0, \Phi/2)$ to generate a pure mode III torsion load, translating into a nominal shear stress, referred to the section having diameter Φ , equal to 1 MPa, except for the

TABLE 3 FE analyses of 3D geometries under mode I, II, and III loadings

Mode I						
Figure	a [mm]	d [mm]	2α [°]	b [mm]	t [mm]	Number of analyses^a
(3A)	1, 2, ..., 9, 10	1	0	—	—	10
(3B)	1, 2, ..., 19, 20	1	0	—	—	20
(3B)	10	2, 5, 10	0	—	—	3
(3C)	5	1, 2, 2.5, 5	90	—	—	4
(3C)	10	1, 2.5, 3, 5, 7.5	90	—	—	5
(3C)	15	1, 2, 5	90, 120	—	—	6
(3C)	5	1, 2, 2.5, 5	120	—	—	4
(3C)	10	1, 2.5, 3, 5, 7.5	120	—	—	5
(3C)	10	1, 2.5, 5, 10	135	—	—	4
(3D)	6.5	0.5, 1, 1.5, 3, 6.5	135	10	8	5
(3D)	50	2, 5, 8, 10	135	50	16	4
Mode II						
Figure	a [mm]	d [mm]	2α [°]	b [mm]	t [mm]	Number of analyses^b
(3E)	3	3	0	—	—	1
(3E)	4	3, 4	0	—	—	2
(3E)	5	3, 4, 5	0	—	—	3
(3E)	6	3, 4, 6	0	—	—	3
(3E)	7	3.5, 7	0	—	—	2
(3E)	8	4, 6, 8	0	—	—	3
(3E)	9	3, 4.5, 6	0	—	—	3
(3E)	10	3, 5, 10	0	—	—	3
(3E)	20	4, 5, 6, 10	0	—	—	4
(3E)	30	3, 5, 7, 10	0	—	—	4
(3E)	40	4, 5, 8, 10	0	—	—	4
(3E)	50	3, 5, 10	0	—	—	3
(3E)	60	3, 4, 5, 8, 10	0	—	—	5
(3E)	70	3.5, 5, 10	0	—	—	3
(3E)	80	4, 5, 8, 10	0	—	—	4
(3E)	90	4.5, 5, 7.5, 10	0	—	—	4
(3E)	100	4, 5, 8, 10	0	—	—	4
Mode III						
Figure	a [mm]	d [mm]	2α [°]	Φ [mm]	I_{sp} [mm]	Number of analyses^c
(3F)	5	1, 2.5, 5	0, 90, 120, 135	50	—	12
(3F)	7	1, 3.5, 7	0, 90, 120, 135	50	—	12
(3F)	10	1, 2.5, 5	0, 90, 120, 135	50	—	12
(3G)	5	5	90, 120, 135	50	—	3
(3G)	10	5, 10	90, 120, 135	50	—	6
(3G)	15	5, 10	90, 120, 135	50	—	6
(3H)	2	2	0	50	4	1
(3H)	5	2.5, 5	0	50	10	2
(3H)	10	2.5, 5	0	50	20	2

^aTotal number of analyses: 70 × 2 element types (TETRA 4 and TETRA 10) = 140 analyses.^bTotal number of analyses: 55 × 2 element types (TETRA 4 and TETRA 10) = 110 analyses.^cTotal number of analyses: 56 × 2 element types (TETRA 4 and TETRA 10) = 112 analyses.

case of Figure 3H for which the applied forces translate to a nominal shear stress equal to 1 MPa only in the case $a = 10$ mm.

After solution, the out-of-plane shear peak stress $\tau_{\theta z, \theta=0, \text{peak}}$ has been evaluated at vertex nodes belonging to the crack or V-notch tip lines (Figure 3F–H), stress averaging at FE nodes being activated as described for mode I FE analyses. Then, Equation (7) has been used to calculate the average peak stress $\bar{\tau}_{\theta z, \theta=0, \text{peak}}$ at each vertex node.

Again, the exact values of the NSIF K_3 , to input in Equation (10), have been calculated by using Ansys Mechanical APDL code and by applying Equation (3) to the stress-distance results derived from two-dimensional FE analyses with very refined FE meshes of eight-node, quadratic quadrilateral harmonic elements (PLANE 83 of Ansys® element library).

5 | DETAILS OF MESH GENERATION SETTINGS

Three-dimensional free mesh patterns consisting of four-node or ten-node tetrahedral elements have been adopted in the FE analyses. Table 2 shows that the four-node tetrahedral element has been integrated using 1 Gauss point, Ansys Mechanical APDL being the only exception since it employs 4 Gauss points; on the other hand, the ten-node tetrahedral element has been integrated using 4 Gauss points by all considered FE codes. To run the free mesh generation algorithm, first, the proper element type has been selected, then, the sole parameter, which the FE analyst has input, has been the average element size d . More details regarding the element type selection and the adopted mesh generation settings in individual FE codes have been summarized in Appendix A.

6 | RESULTS OF FE ANALYSES

Figures 4–6 report the results obtained from the participants in the Round Robin regarding the mode I, mode II, and mode III notch problems, respectively. The results are expressed in terms of the PSM parameters K^*_{FE} , K^{**}_{FE} , and K^{***}_{FE} , defined by Equations (8)–(10), respectively, as a function of the mesh density ratio a/d . It should be noted that, the variability of the average peak stress $\bar{\sigma}_{ij, \text{peak}}$ along the notch or crack tip lines causes a non-uniform distribution of coefficients K^*_{FE} , K^{**}_{FE} and K^{***}_{FE} in each FE model. Therefore, Figures 4–6 report the mean value of the non-dimensional parameters K_{FE} evaluated from each FE model as well as the relevant bar,

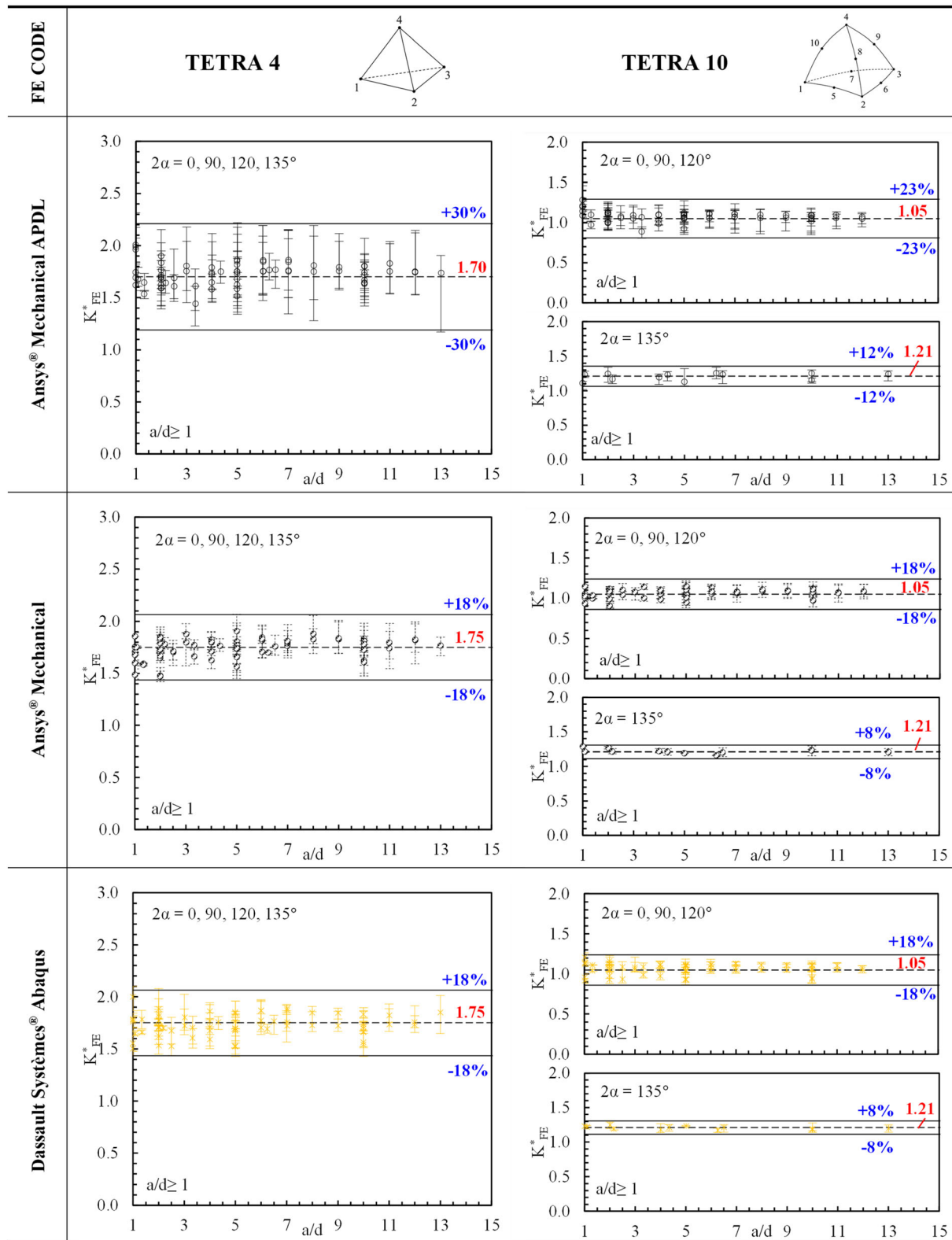
which represents the range between maximum and minimum K_{FE} values evaluated along each notch or crack tip line. In the case of the same FE code adopted by different participants (see for example the number of users of Ansys Mechanical APDL in Table 2), the mean value and the bar of the ratios K_{FE} reported in Figures 4–6 have been calculated collecting together the numerical results of all users. It is worth noting that the results generated by the same FE code adopted by different users are interesting for the present Round Robin, since the mesh pattern generated for a given geometrical case could change depending on the order of creation of the geometrical entities or the performances of the adopted PC. More in detail, if the mean values of the K^*_{FE} parameter evaluated from each FE model were calculated individually for different users adopting the same FE code, the differences would be appreciable, being in most cases between 2% and 10%, but achieving also 20% in 2 cases out of 70. Similar results would be obtained for K^{**}_{FE} and K^{***}_{FE} , the main factor generating these deviations being the order of creation of the geometrical entities. Such differences are taken into account by the bars of the ratios K_{FE} reported in Figures 4–6. Figures 4–6 show that, for a given element type, the majority of the adopted FE software present similar values of the non-dimensional parameters K^*_{FE} , K^{**}_{FE} , and K^{***}_{FE} and of the minimum mesh density ratio a/d for the applicability of the PSM. More in detail, concerning 3D, four-node tetrahedral elements, Figures 4–6 highlight the following:

- Under mode I loading (see Figure 4), K^*_{FE} is in the range between 1.68 and 1.78 for all considered values of the notch opening angle 2α , the deviation being between $\pm 18\%$ and $\pm 30\%$. Convergence is obtained when $a/d \geq 1$.
- Dealing with mode II loading (see Figure 5), K^{**}_{FE} is in the range between 2.63 and 3.00, the deviation being between $\pm 12\%$ and $\pm 18\%$, and convergence is obtained when the ratio $a/d \geq 3$.
- Concerning mode III loading, the obtained results are reported in Figure 6, which shows that K^{***}_{FE} is in the range between 2.35 and 2.60, the deviation being between $\pm 15\%$ and $\pm 23\%$, and convergence is obtained when the ratio $a/d \geq 5$.

Dealing with 3D,

ten
-node tetrahedral elements, Figures 4–6 highlight the following:

- Under mode I loading, Figure 4 show that K^*_{FE} is in the range between 1.05 and 1.07, with a deviation between $\pm 15\%$ and $\pm 23\%$, for 2α equal to 0° , 90° , or

MODE I**FIGURE 4** Results of Round Robin for mode I loading: Non-dimensional parameter K^*_{FE} for all considered FE codes

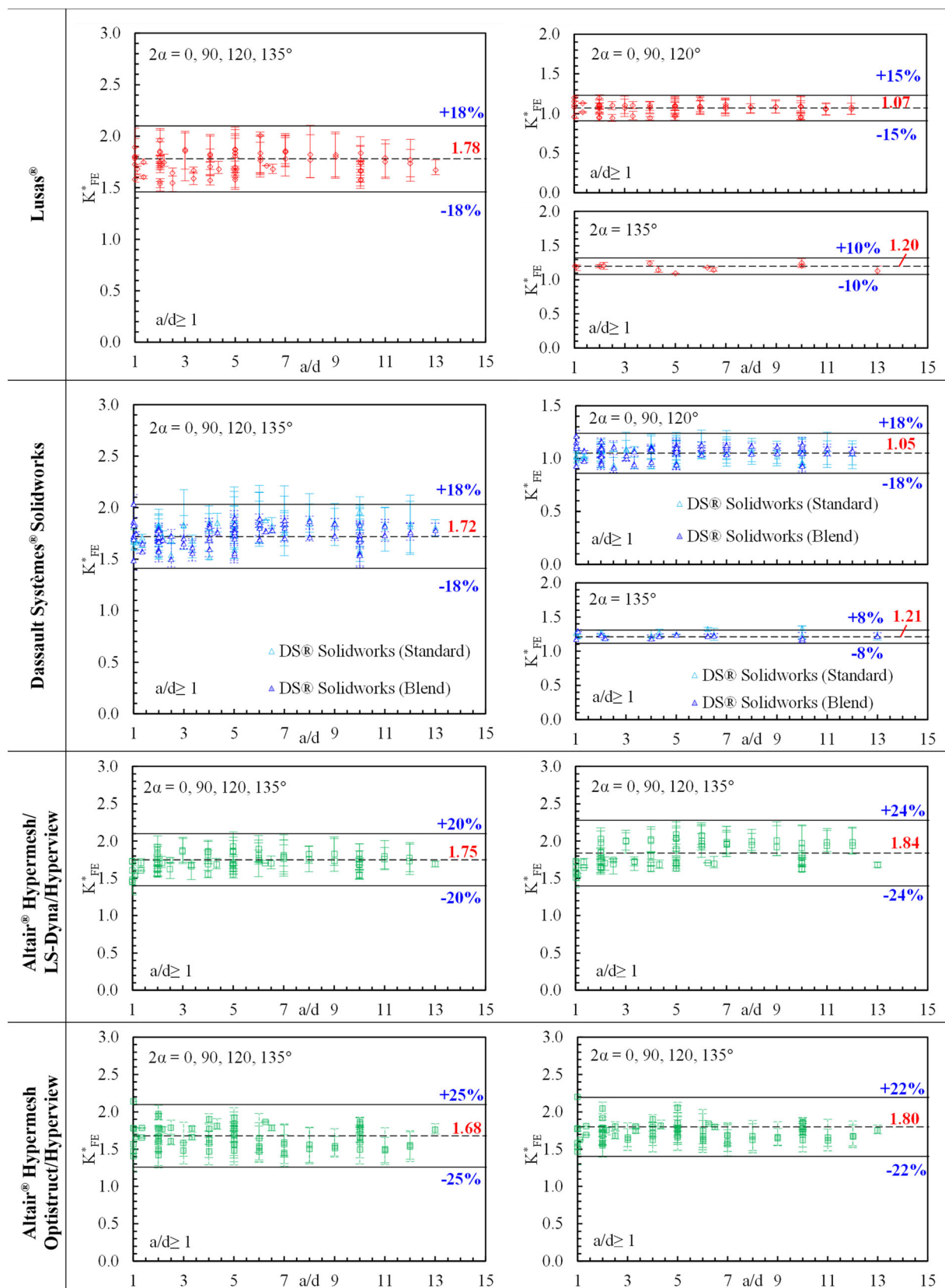


FIGURE 4 (Continued)

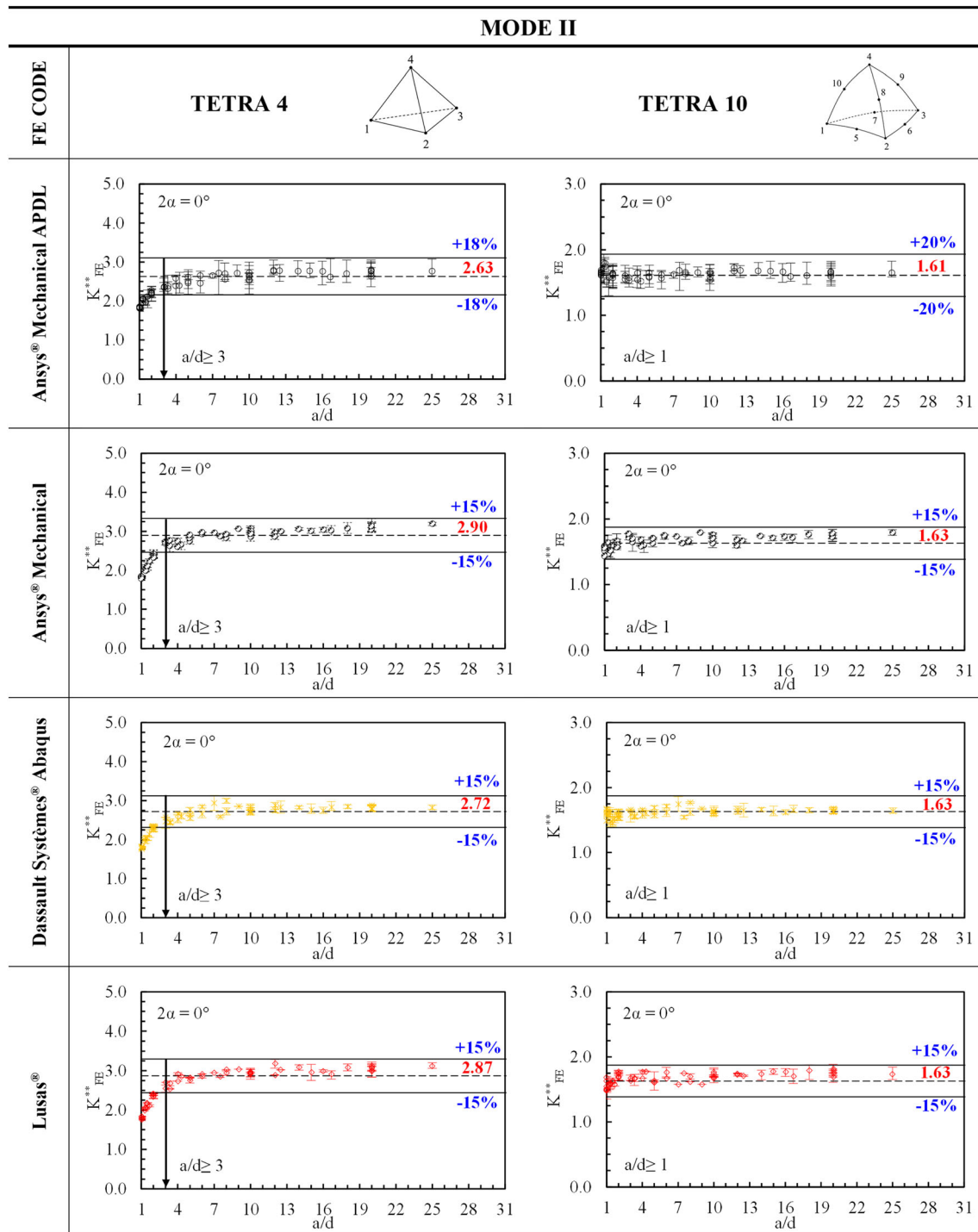


FIGURE 5 Results of Round Robin for mode II loading: Non-dimensional parameter K^{**}_{FE} for all considered FE codes

120° . K^*_{FE} is in the range between 1.20 and 1.21, with a deviation between $\pm 8\%$ and $\pm 12\%$, when 2α equals 135° . The only exceptions are FE packages Hypermesh/LS-Dyna/Hyperview and Hypermesh/Optistruct/Hyperview which present $K^*_{FE} = 1.84 \pm 24\%$ and $1.80 \pm 22\%$, respectively, for all considered values of the notch opening angle 2α . Convergence is obtained when $a/d \geq 1$ for all cases.

- Concerning mode II loading (see Figure 5), K^*_{FE} is in the range between 1.61 and 1.63, with a deviation between $\pm 13\%$ and $\pm 20\%$, while convergence is obtained for a ratio $a/d \geq 1$. Again, the only exceptions are Hypermesh/LS-Dyna/Hyperview and Hypermesh/Optistruct/Hyperview which present a $K^*_{FE} = 2.70 \pm 18\%$ and $2.87 \pm 15\%$ and convergence is obtained when $a/d \geq 3$.

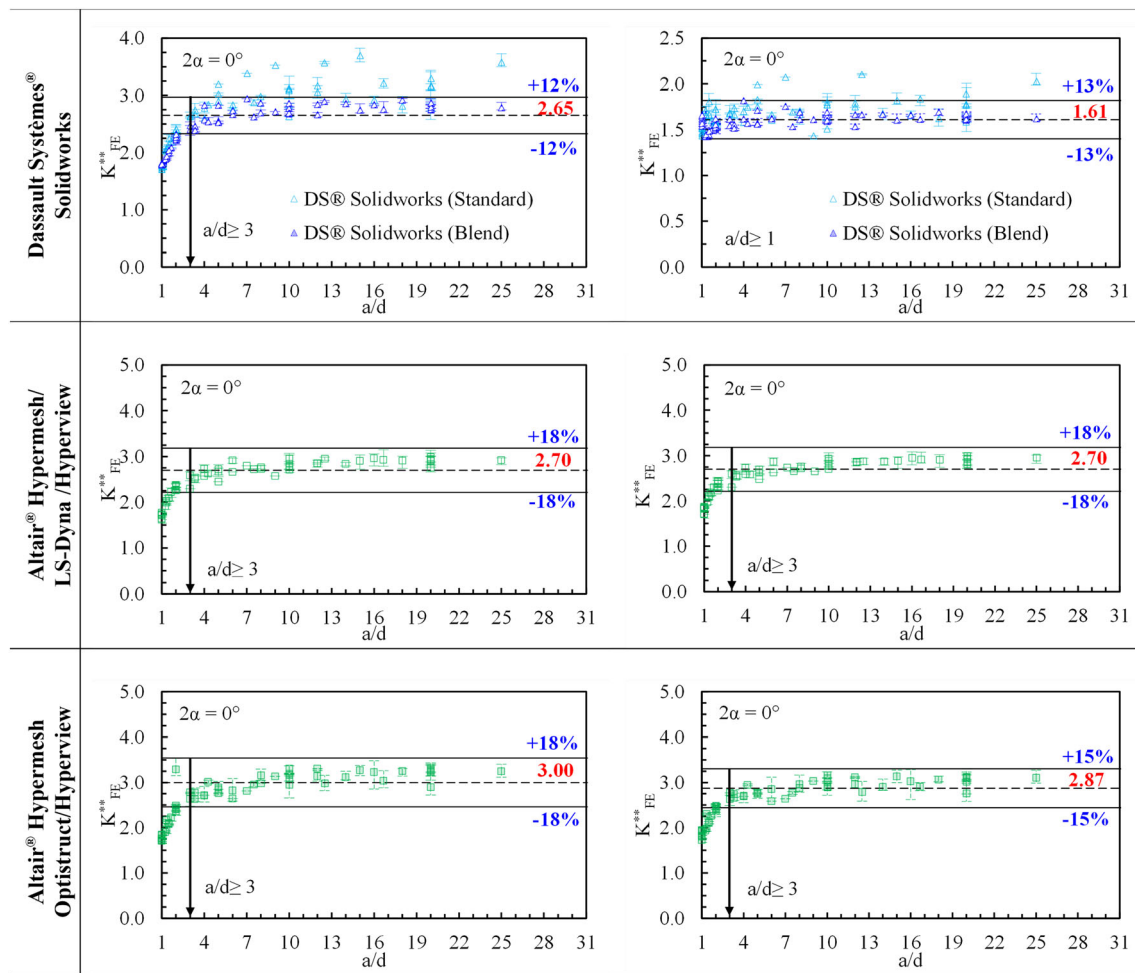


FIGURE 5 (Continued)

- Dealing with mode III loading, Figure 6 show that K^{***}_{FE} is in the range between 1.32 and 1.40, with a deviation between $\pm 10\%$ and $\pm 15\%$, for 2α equal to 0° and 90° , convergence being obtained for a ratio $a/d \geq 3$, the only exception being Abaqus for which it must be $a/d \geq 5$. On the other hand, K^{***}_{FE} is in the range between 1.60 and 1.70, with a deviation between $\pm 10\%$ and $\pm 12\%$, when 2α equals 120° or 135° , convergence being obtained for a ratio $a/d \geq 1$, the only exception being again Abaqus for which it must be $a/d \geq 4$. Once again, Hypermesh/LS-Dyna/Hyperview and Hypermesh/Optistruct/Hyperview present different values of the PSM parameters, namely, $K^{***}_{FE} = 2.45 \pm 15\%$ for $a/d \geq 3$ and $K^{***}_{FE} = 2.50 \pm 18\%$ for $a/d \geq 1$, respectively, for all considered values of the notch opening angle 2α .

Table 4 summarizes all results showed in Figures 4–6, that is, the non-dimensional ratios K^*_{FE} , K^{**}_{FE} , and K^{***}_{FE} to input in Equations (4)–(6) and the minimum

mesh density ratio a/d for individual FE software packages.

Importantly, the PSM parameters K^*_{FE} , K^{**}_{FE} , and K^{***}_{FE} reported here using Ansys Mechanical APDL are slightly different results as compared to the original calibration,⁵⁰ as it can be observed from Table 4. In fact, the mean values of the parameters K_{FE} have been slightly modified and a little greater deviation has to be accepted to take into account the distribution of the results obtained by all users of Ansys Mechanical APDL, due to the different mesh pattern generated for a given geometry; on the other hand, the minimum mesh density ratio a/d to achieve convergence has been reduced. See for example the case of mode I notch problems treated with four-node tetrahedral elements: the original calibration⁵⁰ provided $K^*_{FE} = 1.75 \pm 22\%$ for $a/d \geq 3$, while the present calibration provides $K^*_{FE} = 1.70 \pm 30\%$ for $a/d \geq 1$. However, the scatter obtained for Ansys Mechanical APDL would be in agreement with that obtained here with other FE software packages, if Ansys results were

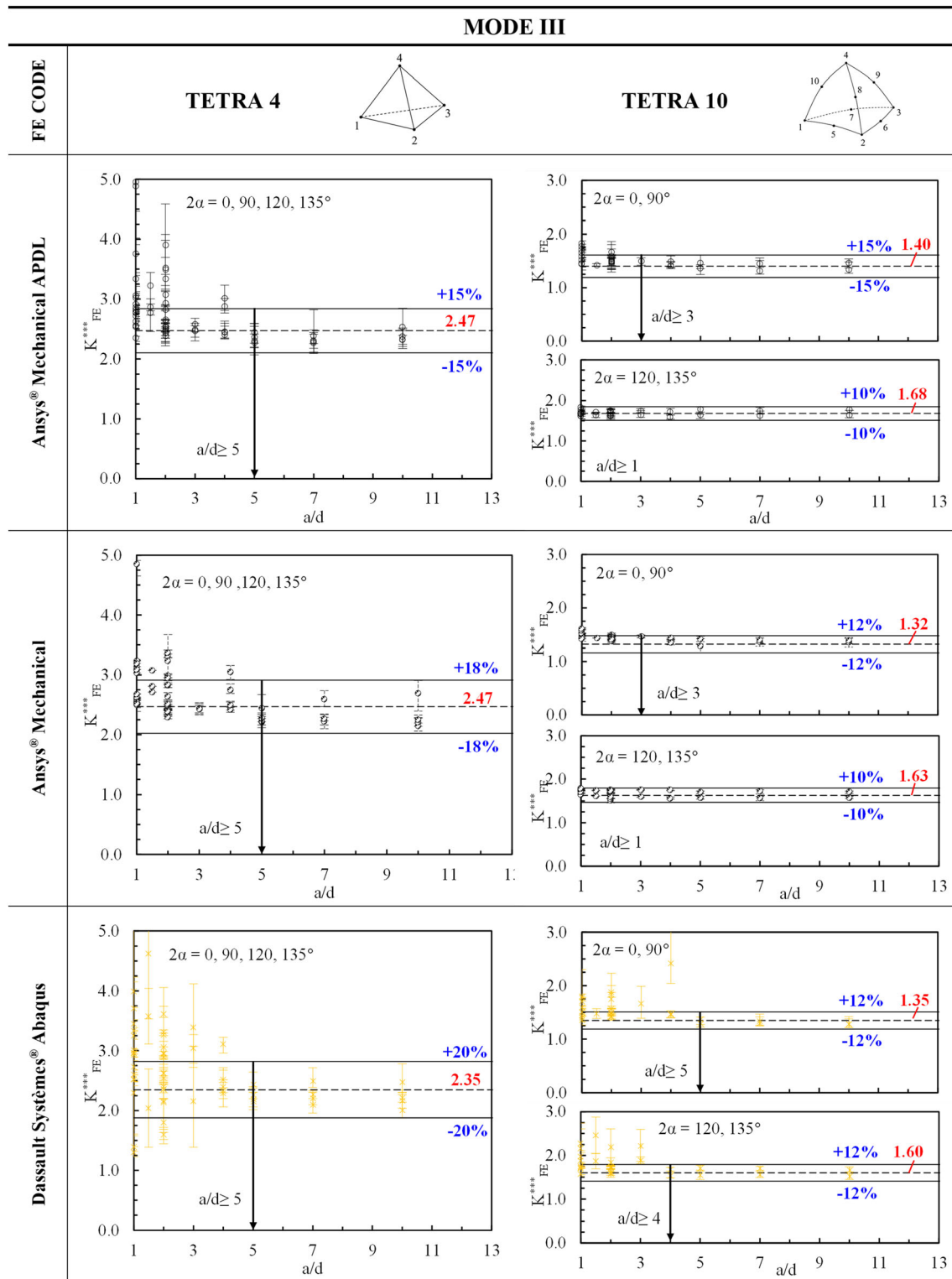


FIGURE 6 Results of Round Robin for mode III loading: Non-dimensional parameter K^{***}_{FE} for all considered FE codes

taken only from the calibration performed by a single user.

Figures 4–6 show that the calibration of the K^*_{FE} , K^{**}_{FE} , and K^{***}_{FE} performed using Solidworks provides

different results as a function of the adopted mesh generation option, that is, *standard* or *blend*. More in detail, results generated using *standard mesh* are highly scattered, especially for mode II crack problems (see

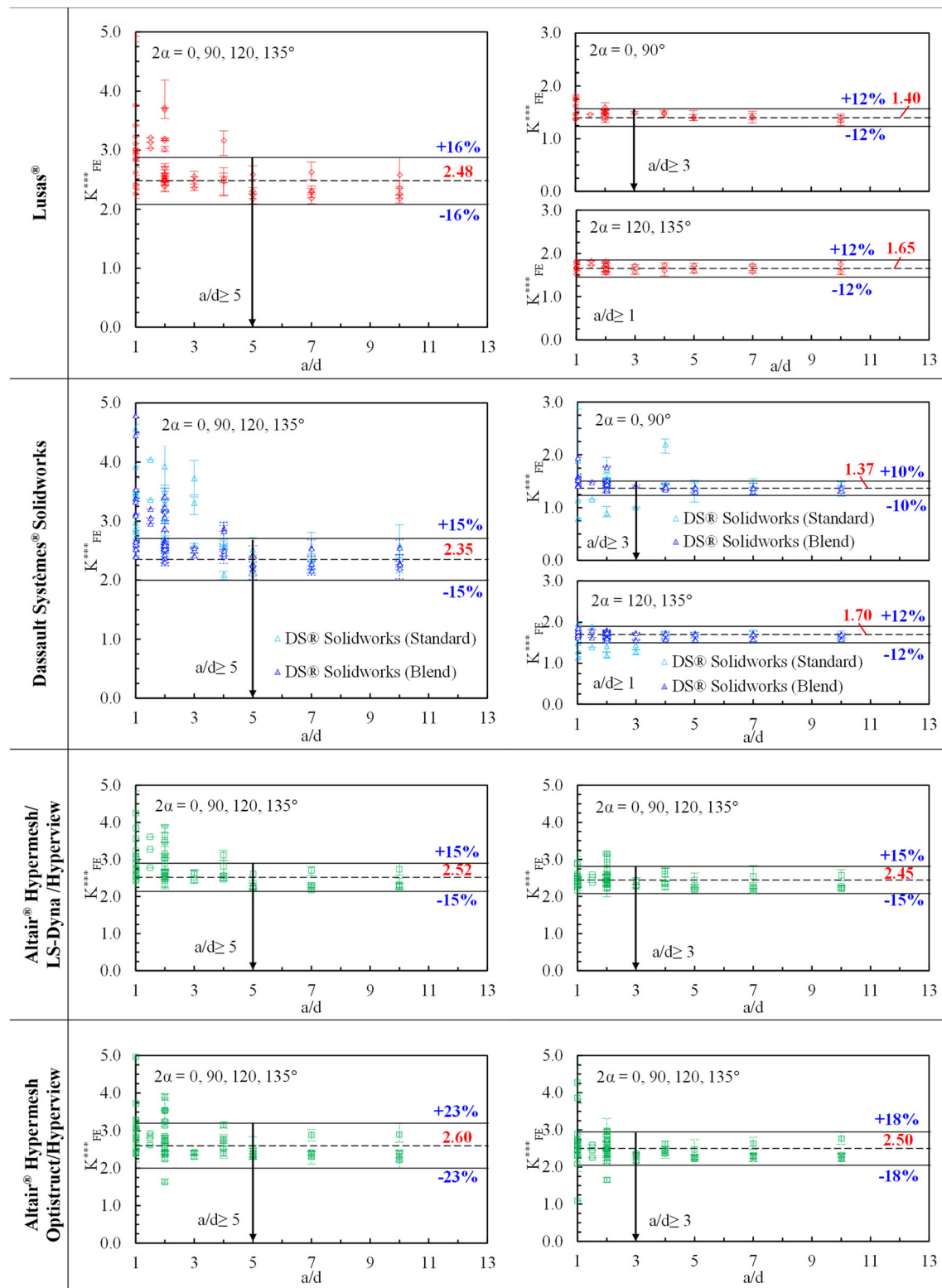


FIGURE 6 (Continued)

Figure 5), while results obtained using a *blend mesh* are consistent with those generated by the other FE codes. This is due to the generated mesh pattern, which is quasi-mapped, consisting of right triangles on the free

surface of the component, for the *standard mesh*, while it is free, that is, made of nearly equilateral triangles, when using the *blend mesh*, as sketched in Table 2. Accordingly, the scatter bands reported in Figures 4–6 and the

TABLE 4 Summary of parameters K^*_{FE} , K^{**}_{FE} , and K^{***}_{FE} and minimum mesh density ratios a/d to apply the PSM with all considered FE codes using either four-node or ten-node tetrahedral elements

Software	PSM parameter	Mode I— K^*_{FE} (Equation 8)				Mode II— K^{**}_{FE} (Equation 9)				Mode III— K^{***}_{FE} (Equation 10)			
		TETRA 4		TETRA 10		TETRA 4		TETRA 10		TETRA 4		TETRA 10	
		0, 90, 120, 135	0, 90, 120	135	0	0	0	0	0	0, 90, 120, 135	0, 90	0, 90, 120, 135	0, 90
Ansys® Mechanical APDL <i>original calibration^{s0}</i>	K_{FE}	1.75 ± 22%	1.05 ± 15%	1.21 ± 10%	2.65 ± 15%	1.63 ± 20%	2.50 ± 15%	1.37 ± 15%	1.70 ± 10%	3	3	3	3
	$(a/d)_{\min}$	3	3	1	3	1	5	5	5				
Ansys® Mechanical APDL	K_{FE}	1.70 ± 30%	1.05 ± 23%	1.21 ± 12%	2.63 ± 18%	1.61 ± 20%	2.47 ± 15%	1.40 ± 15%	1.68 ± 10%	3	3	3	1
	$(a/d)_{\min}$	1	1	1	3	1	5	5	5				
Ansys® Mechanical	K_{FE}	1.75 ± 18%	1.05 ± 18%	1.21 ± 8%	2.90 ± 15%	1.63 ± 15%	2.47 ± 18%	1.32 ± 12%	1.63 ± 10%	1	1	1	1
	$(a/d)_{\min}$	1	1	1	3	1	5	5	5				
Dassault Systèmes® Abaqus	K_{FE}	1.75 ± 18%	1.05 ± 18%	1.21 ± 8%	2.72 ± 15%	1.63 ± 15%	2.35 ± 20%	1.35 ± 12%	1.60 ± 12%	5	5	4	4
	$(a/d)_{\min}$	1	1	1	3	1	5	5	5				
Lusas®	K_{FE}	1.78 ± 18%	1.07 ± 15%	1.20 ± 10%	2.87 ± 15%	1.63 ± 15%	2.48 ± 16%	1.40 ± 12%	1.65 ± 12%	3	3	1	1
	$(a/d)_{\min}$	1	1	1	3	1	5	5	5				
Dassault Systèmes® Solidworks^a	K_{FE}	1.72 ± 18%	1.05 ± 18%	1.21 ± 8%	2.65 ± 12%	1.61 ± 13%	2.35 ± 15%	1.37 ± 10%	1.70 ± 12%	5	5	3	1
	$(a/d)_{\min}$	1	1	1	3	1	5	5	5				
Altair® Hypermesh/ LS-Dyna/Hyperview	K_{FE}	1.75 ± 20%	1.84 ± 24%	1.84 ± 24%	2.70 ± 18%	2.70 ± 18%	2.52 ± 15%	2.45 ± 15%	2.45 ± 15%	3	3	3	3
	$(a/d)_{\min}$	1	1	1	3	3	5	5	5				
Altair® Hypermesh/ Optistruct/Hyperview	K_{FE}	1.68 ± 25%	1.80 ± 22%	1.80 ± 22%	3.00 ± 18%	2.87 ± 15%	2.60 ± 23%	2.50 ± 18%	2.50 ± 18%	1	1	1	1
	$(a/d)_{\min}$	1	1	1	3	3	5	5	5				

^aUsing Blend mesh generation option (see Table 2).

results summarized in Table 4 relevant to Solidworks have been referred only to the *blend mesh*, which is consistent with the mesh patterns generated by the other FE codes, which typically define a free mesh pattern of predominantly equilateral triangles.

Concerning the minimum mesh density ratios, since the PSM relies on the asymptotic stress distribution quantified by the NSIFs, therefore, the greater the extension of the asymptotic stress field starting from the notch tip, the larger the mesh size can be. As an example, in Campagnolo et al.,⁵⁷ it was shown that the more refined FE meshes required by mode III stresses as compared to mode I stresses were due to the smaller extension of the asymptotic stress field under mode III. Moreover, ten-node tetrahedral elements are more accurate, owing to the higher number of nodes and Gauss points as compared to four-node tetrahedral elements, therefore coarser meshes can be adopted, that is, lower mesh density ratios a/d .

Finally, the different calibration constants obtained using Hypermesh/LS-Dyna/Hyperview and Hypermesh/Optistruct/Hyperview, depend on criteria for stress extrapolation at FE nodes and will be discussed in the following section.

7 | DISCUSSION

In previous section, some differences have been observed among the results provided by the adopted FE software packages. The most significant one is highlighted by Figures 4–6 and Table 4 and is that Hypermesh/LS-Dyna/Hyperview and Hypermesh/Optistruct/Hyperview deliver K_{FE} , K^{**}_{FE} , and K^{***}_{FE} values calculated with ten-node tetrahedral elements completely different from those found with all other FE codes. Other minor differences of PSM coefficients provided by the other FE codes

have also been observed. Such discrepancies have been motivated on the basis of the different criteria adopted to extrapolate stresses at FE nodes, of the generated mesh patterns and of the finite element formulations, as reported in more detail in the following sections.

7.1 | Stress extrapolation at FE nodes

Numerical results are calculated by FE software at the Gauss (or integration) points of each finite element. Then, results can be evaluated at nodal or centroidal locations by employing the relevant shape functions. The stress component can be calculated at a node shared by different elements by adopting two criteria, as reported in Figure 7 referred to a node shared by two elements^{69,70}:

- a. The nodal stresses in the element ($\sigma_{ij,k}^{(I)}$ and $\sigma_{ij,k}^{(II)}$ in Figure 7A) are derived by extrapolating the stresses existing at the Gauss points. Then, the nodal stresses per element are averaged to compute the stress component at the node ($\sigma_{ij,k}$ in Figure 7A):

$$\begin{aligned}\sigma_{ij,k} &= \frac{\sigma_{ij,k}^{(I)} + \sigma_{ij,k}^{(II)}}{2} \text{ or in the general case } \sigma_{ij,k} \\ &= \frac{\sum_{n=1}^N \sigma_{ij,k}^{(n)}}{N} \text{ where } N = \text{FEs sharing node } k\end{aligned}\quad (11)$$

- b. The centroidal stresses in the element ($\sigma_{ij,c}^{(I)}$ and $\sigma_{ij,c}^{(II)}$ in Figure 7B) are derived by interpolating the stresses existing at the Gauss points and, then, they are attributed to the shared node. Afterwards, they are averaged to compute the stress component at the shared node ($\sigma_{ij,k}$ in Figure 7B):

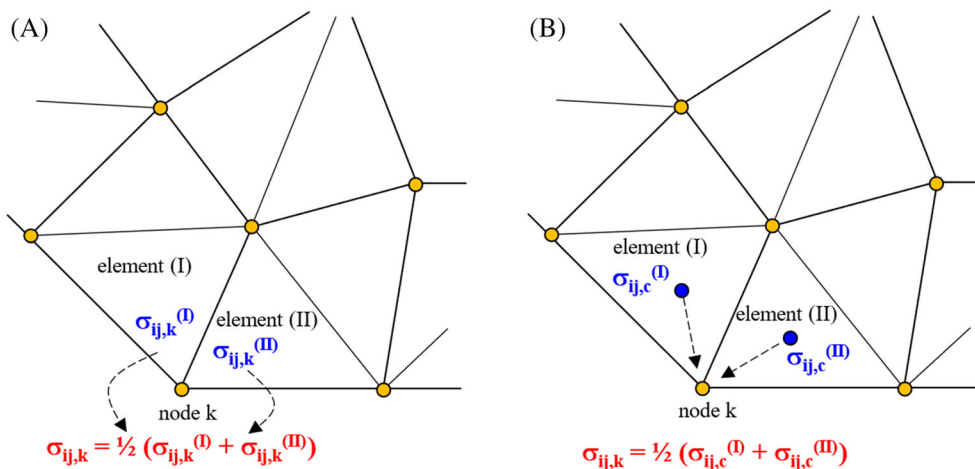


FIGURE 7 Stress extrapolation at FE nodes based on (A) nodal stresses or (B) centroidal stresses. See also previous work⁴⁸ [Colour figure can be viewed at wileyonlinelibrary.com]

$$\sigma_{ij,k} = \frac{\sigma_{ij,c}^{(I)} + \sigma_{ij,c}^{(II)}}{2} \text{ or in the general case } \sigma_{ij,k} \\ = \frac{\sum_{n=1}^N \sigma_{ij,c}^{(n)}}{N} \text{ where } N = \text{FEs sharing node } k \quad (12)$$

The procedure sketched in Figure 7A and defined in Equation (11) is applied by the great majority of the adopted FE codes, that is, Ansys, Abaqus, Lusas, and Solidworks. On the other hand, the postprocessor Hyperview allows to apply either Equation (11) or Equation (12); however, both solvers LS-Dyna and Optistruct do not compute nodal stresses in the element, therefore Hyperview can apply only procedure of Figure 7B and Equation (12) for stress extrapolation at nodes. This explains why the PSM parameters K_{FE}^* , K_{FE}^{**} , and K_{FE}^{***} delivered by LS-Dyna and Optistruct are different from those derived using the other FE software packages, as highlighted in Figures 4–6 and in Table 4. This conclusion has been validated by recalibrating the coefficients K_{FE}^* , K_{FE}^{**} , and K_{FE}^{***} using Ansys Mechanical APDL FE code, but enforcing the use of Equation (12) to extrapolate stresses at FE nodes. The obtained results are reported in Figure 8, which includes also the results previously generated by LS-Dyna and Optistruct (Figures 4–6) and the scatter bands calibrated on LS-dyna results. Figure 8 shows that enforcing Equation (12), Ansys Mechanical APDL FE software provides K_{FE} values consistent with those obtained using Hypermesh/LS-Dyna/Hyperview and Hypermesh/Optistruct/Hyperview.

7.2 | Principal stress averaging

When considering a pure opening (mode I) notch problem, the PSM can be applied through Equation 4 by adopting the maximum principal stress $\sigma_{11,\text{peak}}$, which is approximately equal to the opening peak stress $\sigma_{00,0=0,\text{peak}}$ but easier to evaluate, because it does not require a properly aligned cylindrical coordinate system.

Starting from the nodal stress tensors per element calculated with any criterion mentioned previously (Equation 11 or Equation 12), the principal stresses at a node shared by different finite elements can be evaluated according to two averaging procedures, as sketched in Figure 9 for a node shared by two elements:

- The nodal stress tensors per element ($[\sigma]_k^{(I)}$ and $[\sigma]_k^{(II)}$ in Figure 9A) are averaged at the share node ($[\sigma]_k$ in Figure 9A). Then, the nodal principal stress is evaluated ($\sigma_{11,k}$ in Figure 9A).
- The nodal principal stress per element ($\sigma_{11,k}^{(I)}$ and $\sigma_{11,k}^{(II)}$ in Figure 9B) is calculated from the relevant

nodal stress tensors per element ($[\sigma]_k^{(I)}$ and $[\sigma]_k^{(II)}$ in Figure 9B). Afterwards, nodal principal stress ($\sigma_{11,k}$ in Figure 9B) is obtained by averaging the nodal principal stresses per element at the shared node ($\sigma_{11,k}$ in Figure 9B).

Table 5 summarizes the nomenclature, where available, used by each FE software to define procedures (a) and (b) for principal stress averaging, according to Figure 9. The table reports also the *default option* adopted by individual FE codes and it is seen that option (a) is the default for Ansys, Lusas and Solidworks, while option (b) is the default for Abaqus and the post-processor Hyperview.

To investigate the effects of options (a) and (b) on K_{FE}^* value to be adopted in Equation (4), the mode I problems of Figure 3A–D have been re-analyzed with Ansys Mechanical APDL FE code, but now calculating the maximum principal stress $\sigma_{11,\text{peak}}$, using either option (a) or (b) of Figure 9, instead of the opening peak stress $\sigma_{00,0=0,\text{peak}}$. The obtained results are reported in Figure 9C–F, which show that the mean values of K_{FE}^* are all inside the scatter bands previously calibrated using the opening peak stress $\sigma_{00,0=0,\text{peak}}$ (Figure 4), regardless the procedure adopted for principal stress averaging. However, Figure 9C–F show that when using procedure (b), the resulting K_{FE}^* values are on average well below the mean value of K_{FE}^* reported in Figure 4.

7.3 | FE mesh pattern

When analyzing a given geometry with the same average element size d , the FE software packages generate different FE mesh patterns.

The influence of different FE meshes has been analyzed by considering as case study the mode I problem of Figure 3D, that is, a full-penetration cruciform welded joint under axial loading, having thickness $2a = 13$ mm, notch opening angle at the weld toe $2\alpha = 135^\circ$ and global element size $d = 3$ mm. The mesh patterns generated by all considered FE codes are reported in Figure 10A–G. Discrepancies in the mesh patterns can be noted from visual inspection of Figure 10A–G; therefore, a more detailed analysis has been performed to allow a quantitative comparison. Figure 10H reports the number of finite elements that share each vertex node belonging to the weld toe line and show that it is highly scattered, being in the range between 6 (at free surface) and 24, and it has a different trend for different mesh patterns. Figure 10I reports the size of finite elements, that is, the length of the tetrahedron edges, that share each vertex node belonging to the weld toe line. The figure reports the

mean size of the elements along with the relevant bar, which represents the range between maximum and minimum sizes evaluated at each node. Figure 10I shows that the average element size closely matches the nominal

one for Ansys and Abaqus, while it is always larger for Lusas, LS-dyna and Optistruct and always smaller for Solidworks. Moreover, the element size has a strong variability in the range between $0.55 \cdot d_{\text{nom}}$ and $1.85 \cdot d_{\text{nom}}$.

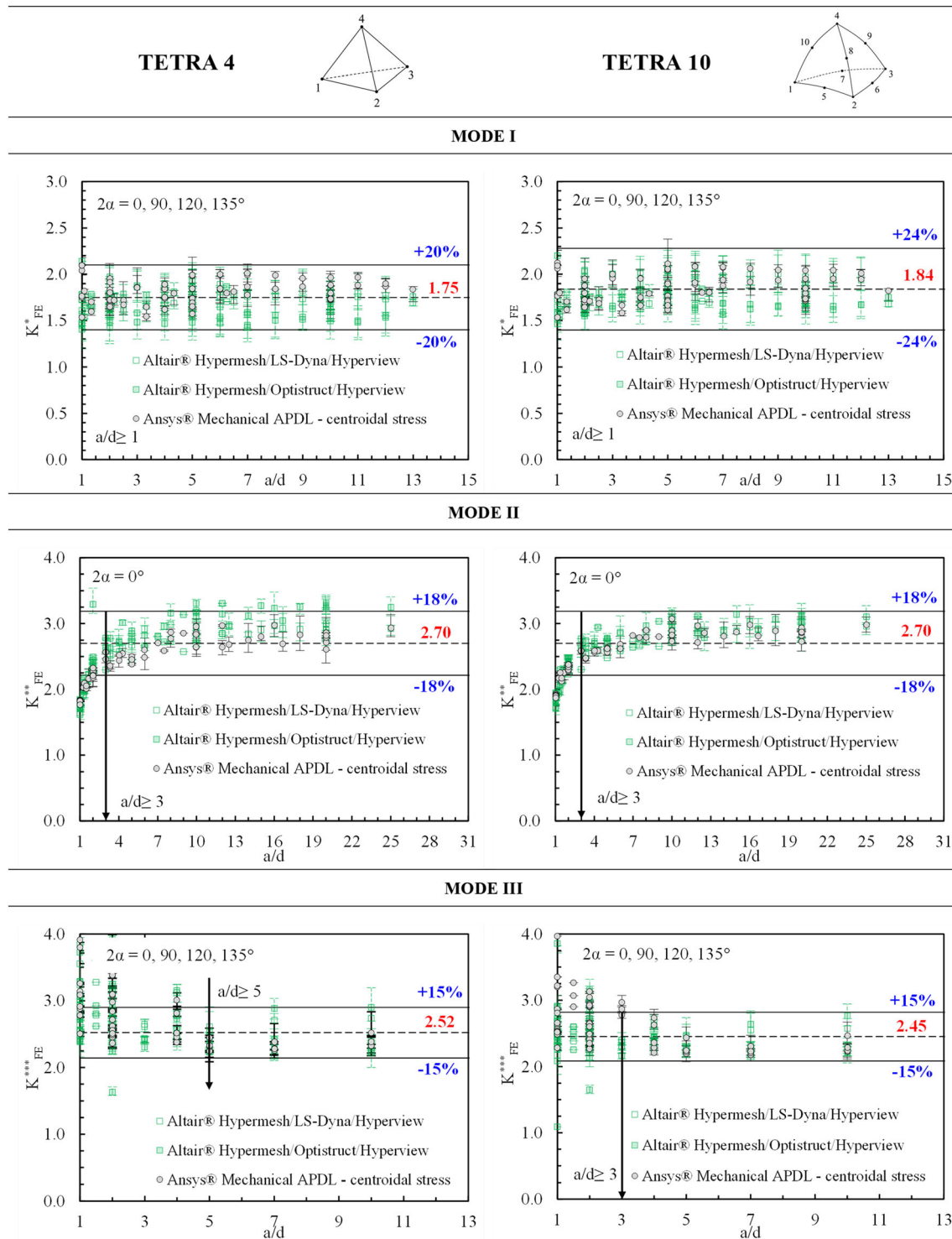


FIGURE 8 Non-dimensional parameters K^*_{FE} , K^{**}_{FE} , and K^{***}_{FE} for Ansys® Mechanical APDL and for Altair® Hypermesh/LS-Dyna/Hyperview and Hypermesh/Optistruct/Hyperview FE packages. Results for mode I, II and III loadings based on centroidal stresses (according to Figure 7B). The scatter bands have previously been calibrated in Figures 4–6 on LS-dyna results [Colour figure can be viewed at wileyonlinelibrary.com]

The great differences in the mesh patterns highlighted in Figure 10H,I, only slightly affect the peak stress distributions. Indeed, Figure 10L,M shows that the mesh patterns of four-node and ten-node tetrahedral elements provide an opening peak stress in the range 0.944–1.197

and 1.417–1.763 MPa, respectively, when considering FE codes which apply Equation (11) to extrapolate stresses at nodes. Despite the strong variability of both the number of finite elements sharing a node and the finite element size above mentioned, the effects on the peak stress

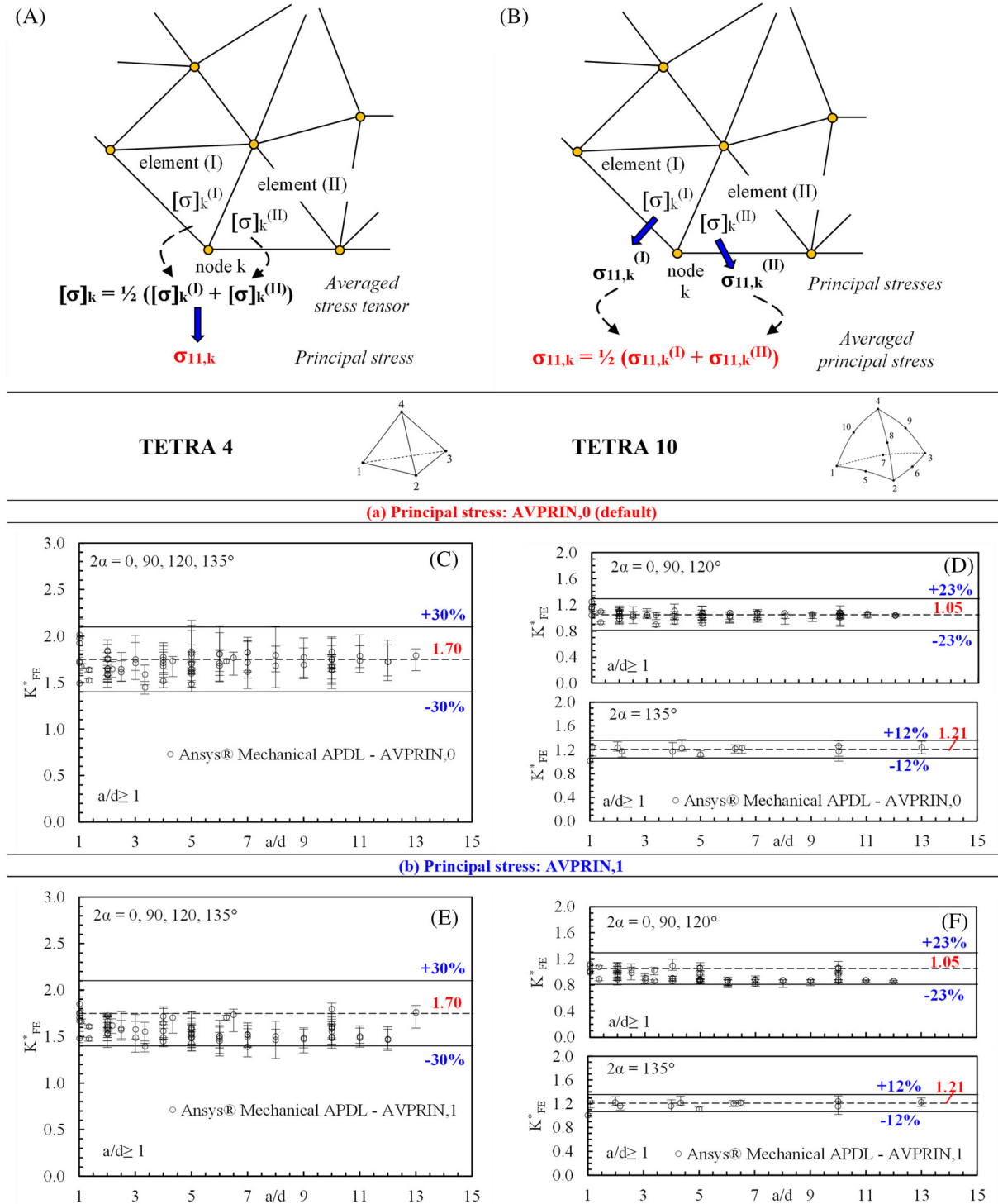


FIGURE 9 Principal stress averaging options. (A) Principal stresses from average stress tensor. (B) Principal stresses from element principal stresses. Non-dimensional parameter K^*_{FE} for Ansys® mechanical APDL. Results for mode I loading obtained by adopting principal stress averaging option (a) in (C), (D) and option (b) in (E), (F). The scatter bands have previously been calibrated in Figure 4 using the opening peak stress $\sigma_{00,0} = \sigma_{0,peak}$ [Colour figure can be viewed at wileyonlinelibrary.com]

TABLE 5 Options for principal stress averaging available in the considered FE codes

FE software	Averaging option (a) of Figure 9	Averaging option (b) of Figure 9
Ansys® Mechanical APDL	AVPRIN,0 or “from components” (default)	AVPRIN,1 or “from principals”
Ansys® Mechanical	default	not available
Dassault Systèmes® Abaqus	“compute scalars after averaging”	“compute scalars before averaging” (default)
Lusas®	Averaged nodal (default)	not available
Dassault Systèmes® Solidworks	default	not available
Altair® Hypermesh/ Hyperview ^a	Averaging method: “Advanced”	Averaging method: “Simple” (default)

^aPost-processor adopted to calibrate both Altair® LS-Dyna and Altair® Optistruct.

distribution are reduced and are demonstrated by the relatively reduced deviations of the K_{FE} parameters in the range between $\pm 8\%$ and $\pm 30\%$.

7.4 | Finite element formulation

All FE codes involved in the present Round Robin integrate four-node and ten-node tetrahedral elements by using 1 and 4 Gauss points, respectively, Ansys Mechanical APDL being the only exception since it adopts 4 Gauss points also for the four-node tetrahedral element, as reported in Table 2.

To analyze the effect of different finite element formulations, the 3D mode I problem of the full-penetration cruciform welded joint reported in Figure 3D has been taken again as a case study. The effect of the FE mesh has been excluded by generating two mesh patterns, one using four-node tetrahedral and the other using ten-node tetrahedral elements, and adopting in both cases the free mesh generation algorithm available in Solidworks with *blend* option activated (see Figure 10E).

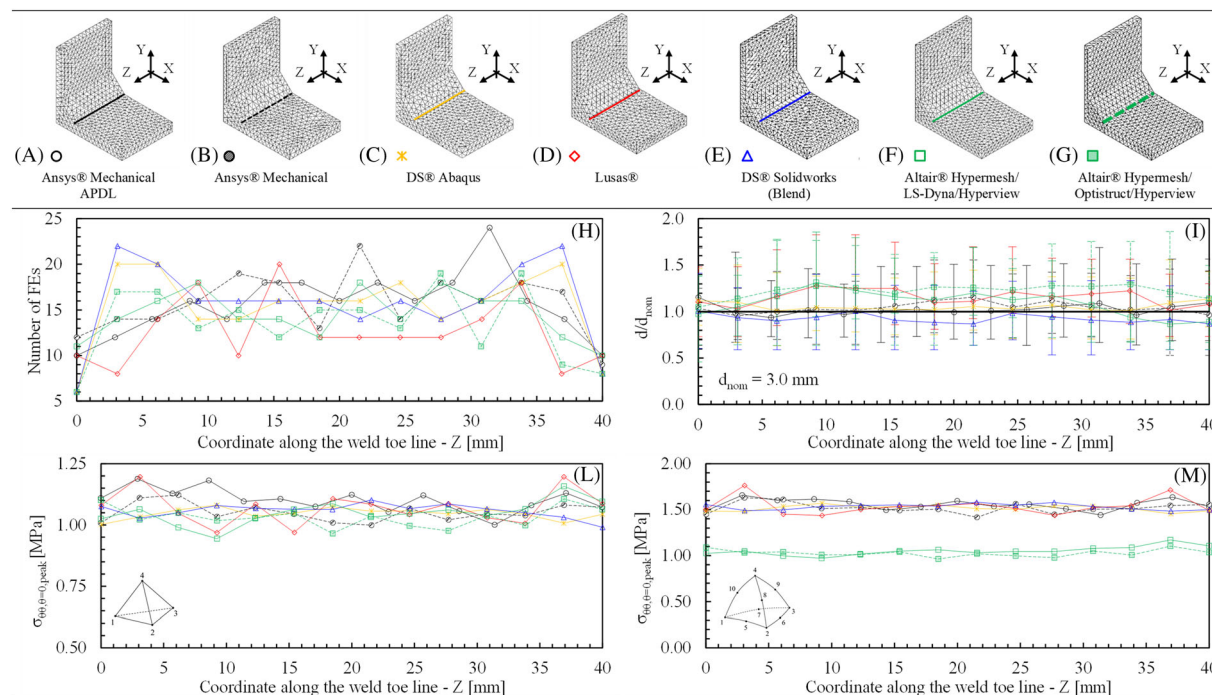


FIGURE 10 FE mesh patterns relevant to the case of Figure 3D with $2a = 13$ mm, $2\alpha = 135^\circ$, and $d = 3$ mm, as obtained with: (A) Ansys Mechanical APDL, (B) Ansys Mechanical, (C) Abaqus, (D) Lusas, (E) Solidworks, (F) Hypermesh/LS-Dyna/Hyperview, and (G) Hypermesh/Optistruct/Hyperview. (H) Number of finite elements that share each vertex node at the weld toe. (I) Normalized size of finite elements that share each vertex node at the weld toe. Comparison of peak stress distributions calculated by all considered FE codes along the weld toe line of the FE models reported in (A)–(G) using (L) four-node and (M) ten-node tetrahedral elements [Colour figure can be viewed at wileyonlinelibrary.com]

Afterwards, the mesh patterns have been imported into all other FE codes to keep identical FE meshes in all analyses.

The obtained results in terms of opening peak stress $\sigma_{\theta=0, \text{peak}}$, evaluated at the vertex nodes belonging to the weld toe line (z direction in Figure 10E), are reported in Figure 11A,B for four-node and ten-node tetrahedral elements, respectively. Figure 11A shows that the peak stress values are perfectly matching for all FE codes, which adopt 1 Gauss point to integrate the four-node

tetrahedral element, even for LS-Dyna and Optistruct, since the centroid coincides with the sole Gauss point. On the other hand, Ansys Mechanical APDL, which adopts 4 Gauss points, delivers different results and on average slightly higher than those calculated by the other FE codes. Figure 11B illustrates a perfect match of the ten-node tetrahedral elements available in all FE codes involved in the present Round Robin, with the only exceptions of LS-Dyna and Optistruct, as it was expected since all codes adopt 4 Gauss points. Moreover,

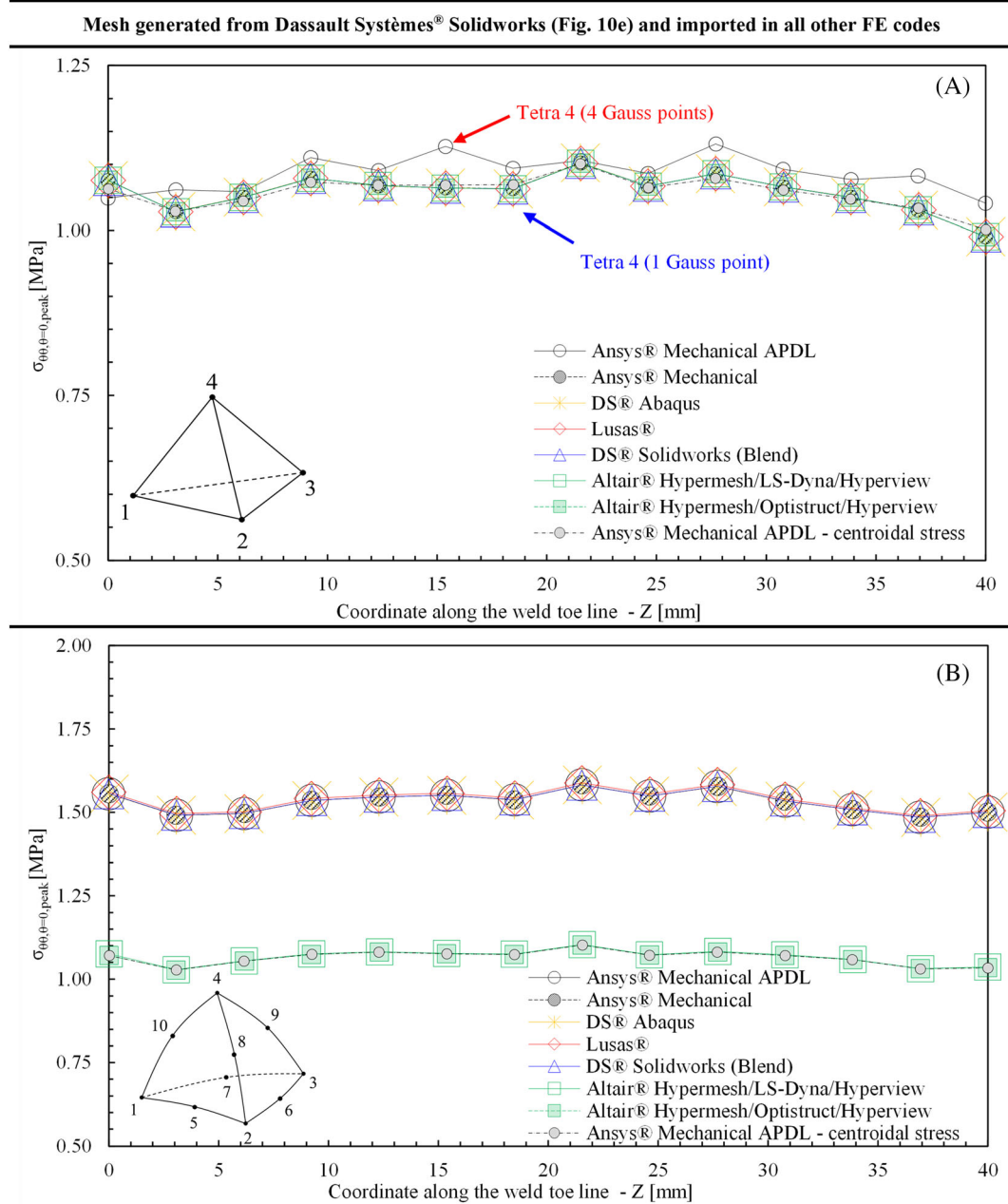


FIGURE 11 Comparison of peak stress distributions calculated by all considered FE codes along the weld toe line of the FE mesh pattern relevant to the case of Figure 3D with $2a = 13$ mm, $2\alpha = 135^\circ$, and $d = 3$ mm, as generated by Solidworks (see Figure 10E) adopting (A) four-node and (B) ten-node tetrahedral elements, respectively [Colour figure can be viewed at wileyonlinelibrary.com]

Figure 11B confirms once again that Ansys Mechanical APDL, when Equation (12) is enforced to extrapolate stresses at FE nodes, provides results coincident with those generated by LS-Dyna and Optistruct, provided that also the mesh pattern and the element formulation are kept the same.

8 | CONCLUSIONS

A Round Robin activity has been performed to calibrate the PSM adopting different FE software packages for a range of coarse three-dimensional FE meshes. The PSM is an engineering, numerical tool originally calibrated using Ansys Mechanical APDL FE code to evaluate rapidly the mode I, II and III linear elastic Notch Stress Intensity Factors (NSIFs); to this aim, the PSM employs the linear elastic opening, in-plane shear and out-of-plane shear peak stresses, respectively, evaluated at the sharp V-notch tip. Three non-dimensional parameters are required to apply the PSM, namely, K_{FE}^* (Equation 4), K_{FE}^{**} (Equation 5), and K_{FE}^{***} (Equation 6), which have been calibrated here adopting four-node and ten-node tetrahedral finite elements available in commercial FE codes, namely Ansys Mechanical APDL, Ansys Mechanical, Abaqus, Lusas, Solidworks, Hypermesh/LS-Dyna/Hyperview, and Hypermesh/Optistruct/Hyperview. All in all, 362 3D FE analyses have been performed for each of the 16 different combinations of FE codes and participants, resulting in 5792 total number of analyses performed. The following conclusions can be drawn:

- The PSM parameters K_{FE}^* , K_{FE}^{**} , and K_{FE}^{***} and the minimum mesh density ratios a/d to guarantee their convergence within a given scatter, result to be dependent on the FE code, element type, notch opening angle and procedure to calculate stresses at FE nodes.
- The main sources of discrepancy among the PSM parameters calculated with the different FE codes are (i) the different methods adopted to extrapolate stresses at FE nodes according to Equation (11) or (12); (ii) the different mesh pattern generated, in terms of number of elements sharing a node and actual finite element size for the same input size given by the FE analyst.
- Additional differences among the considered FE software packages, which affects the results to some extent, include (i) the finite element formulation, in terms of number of Gauss points and (ii) the numerical procedure adopted for principal stress averaging at FE nodes, which is relevant in some particular cases illustrated in the paper. However, the effects of such

differences are taken up by the scatter bands defined for the PSM parameters.

- 3D mesh patterns being coarse and post-processing the evaluated peak stresses being rather rapid and simple, the 3D PSM based on tetrahedral elements seems useful for engineers involved in structural FE analyses of components weakened by sharp V-shaped notches, even when large-scale and geometrically complex structures are investigated.

ACKNOWLEDGMENTS

The Round Robin was conceived and conducted by the Working Group on “Joining Techniques” of the Italian Scientific Association for Stress Analysis (AIAS). The previous effort of all participants is gratefully acknowledged.

AUTHOR CONTRIBUTIONS

Conceptualization, G.Me. and A.Ca.; methodology, G.Me. and A.Ca.; software, G.Me., A.Ca., A.V., M.A., M.B., A.B., D.C., A.Ch., L.C., M.D.A., A.D.L., E.D., S.F., V.F., F.F., A.G., G.Ma., F.M., A.Pa., A.Pi., A.R., A.Sc., R.S., A.Sp., B.Z.; data curation, G.Me., A.Ca. and A.V.; writing—original draft preparation, G.Me. and A.Ca.; writing—review and editing, G.Me., A.Ca., A.V., M.A., M.B., A.B., D.C., A.Ch., L.C., M.D.A., A.D.L., E.D., S.F., V.F., F.F., A.G., G.Ma., F.M., A.Pa., A.Pi., A.R., A.Sc., R.S., A.Sp., B.Z.; visualization, A.Ca., A.V.; supervision, G.Me. All authors have read and agreed to the published version of the manuscript.

DATA AVAILABILITY STATEMENT

The data that support the findings of this study are available from the corresponding author upon reasonable request.

NOMENCLATURE

a	characteristic dimension of a sharp V-notch, that is, the minimum between the notch depth and the ligament size
d	element size of a coarse mesh pattern to apply the peak stress method (PSM)
E	material Young's modulus
K_1, K_2, K_3	notch stress intensity factors (NSIFs) relevant to mode I, II, and III loadings
$K_{FE}^*, K_{FE}^{**}, K_{FE}^{***}$	non-dimensional parameters to estimate K_1 , K_2 , and K_3 by using the peak stress method (PSM)
r, θ, z	cylindrical coordinates
U_r, U_θ, U_z	displacement components in the cylindrical coordinate system
U_x, U_y, U_z	displacement components in the Cartesian coordinate system
x, y, z	Cartesian coordinates

SYMBOLS

2α	opening angle of the considered sharp V-notch
$\lambda_1, \lambda_2, \lambda_3$	stress singularity degrees relevant to mode I, II, and III loadings
ν	material Poisson's ratio
$\sigma_{11,\text{peak}}$	singular, linear elastic, maximum principal stress computed at the sharp V-notch tip by FE analysis according to the PSM
$\sigma_{ij,c}^{(I)}$	centroidal stress component, where $I = \text{finite element number}$
$\sigma_{ij,k}^{(I)}$	nodal stress component, where $k = \text{node number}$, $I = \text{finite element number}$
$\sigma_{ij,k}$	nodal stress component, where $k = \text{node number}$
$\bar{\sigma}_{ij,\text{peak}}$	moving average of the peak stresses computed on three adjacent vertex nodes of a FE mesh consisting of tetrahedral elements
$\sigma_{rr}, \sigma_{00}, \tau_{r0}$	normal and in-plane shear stress components in a cylindrical reference system
$\sigma_{00,0=0, \text{peak}}$	singular, linear elastic, opening (mode I) peak stress computed at the sharp V-notch tip by FE analysis according to the PSM
$\tau_{r0,0=0, \text{peak}}$	singular, linear elastic, in-plane shear (mode II) peak stress computed at the sharp V-notch tip by FE analysis according to the PSM
τ_{rz}, τ_{0z}	out-of-plane shear stress components in a cylindrical reference system
$\tau_{0z,0=0, \text{peak}}$	singular, linear elastic, anti-plane shear (mode III) peak stress computed at the sharp V-notch tip by FE analysis according to the PSM
$[\sigma]_k^{(I)}$	nodal stress tensor, where $k = \text{node number}$, $I = \text{finite element number}$
$[\sigma]_k$	stress tensor, where $k = \text{node number}$

ABBREVIATIONS

FEM	Finite element method
LEFM	Linear elastic fracture mechanics
NSIF	Notch stress intensity factor
PSM	Peak stress method
SED	Strain energy density
SIF	Stress intensity factor
TCD	Theory of critical distances

ORCID

- Giovanni Meneghetti  <https://orcid.org/0000-0002-4212-2618>
- Alberto Campagnolo  <https://orcid.org/0000-0001-8685-6210>
- Alberto Visentin  <https://orcid.org/0000-0002-0674-0443>
- Matteo Benedetti  <https://orcid.org/0000-0001-9158-2429>
- Davide Castagnetti  <https://orcid.org/0000-0003-3300>

5716

- Andrea Chiocca  <https://orcid.org/0000-0002-1472-4398>
- Luca Collini  <https://orcid.org/0000-0002-1497-9470>
- Francesco Frendo  <https://orcid.org/0000-0002-7472-4664>
- Alessandro Greco  <https://orcid.org/0000-0002-5856-5704>
- Alessandro Scattina  <https://orcid.org/0000-0001-8035-7488>
- Raffaele Sepe  <https://orcid.org/0000-0002-1089-4541>

REFERENCES

1. Eurocode 3. *Eurocode 3: Design of Steel Structures—Part 1-9: Fatigue*. CEN; 2005.
2. Hobbacher AF. Recommendations for fatigue design of welded joints and components. In: *IIW Collection*. Springer International Publishing; 2016. Epub ahead of print 2016. doi: 10.1007/978-3-319-23757-2
3. Fricke W. Fatigue analysis of welded joints: state of development. *Mar Struct*. 2003;16:185-200.
4. Bruder T, Störzel K, Baumgartner J, Hanselka H. Evaluation of nominal and local stress based approaches for the fatigue assessment of seam welds. *Int J Fatigue*. 2012;34:86-102.
5. Poutiainen I, Marquis G. A fatigue assessment method based on weld stress. *Int J Fatigue*. 2006;28:1037-1046.
6. Poutiainen I, Tanskanen P, Marquis G. Finite element methods for structural hot spot stress determination—a comparison of procedures. *Int J Fatigue*. 2004;26:1147-1157.
7. Niemi E, Fricke W, Maddox SJ. *Structural Hot-spot Stress Approach To Fatigue Analysis of Welded Components—Designer's Guide*. Singapore: Springer Singapore; 2018 Epub ahead of print 2018. doi:10.1007/978-981-10-5568-3
8. Baumgartner J. Review and considerations on the fatigue assessment of welded joints using reference radii. *Int J Fatigue*. 2017;101:459-468.
9. Baumgartner J, Schmidt H, Ince E, Melz T, Dilger K. Fatigue assessment of welded joints using stress averaging and critical distance approaches. *Weld World*. 2015;59:731-742.
10. Radaj D, Sonsino CM, Fricke W. *Fatigue Assessment of Welded Joints by Local Approaches*. 2nd ed. Cambridge: Woodhead Publishing; 2006.
11. Fricke W. *IIW Recommendations for the Fatigue Assessment of Welded Structures by Notch Stress Analysis: IIW-2006-09*. Woodhead Pub; 2012 Accessed August 22, 2018. <https://www.sciencedirect.com/book/9780857098559/iiw-recommendations-for-the-fatigue-assessment-of-welded-structures-by-notch-stress-analysis>
12. Leitner M, Stoschka M, Ottersböck M. Fatigue assessment of welded and high frequency mechanical impact (HFMI) treated joints by master notch stress approach. *Int J Fatigue*. 2017;101:232-243.
13. Remes H, Gallo P, Jelovica J, Romanoff J, Lehto P. Fatigue strength modelling of high-performing welded joints. *Int J Fatigue*. 2020;135:105555.
14. Shams E, Vormwald M. Fatigue of weld ends under combined loading. *Int J Fatigue*. 2017;100:627-638.
15. Shams E, Malikoutsakis M, Savaidis G, Vormwald M. Notch stress and fracture mechanics based assessment of fatigue of

- seam weld ends under shear loading. *Fatigue Fract Eng Mater Struct.* 2014;37:740-750.
16. Yıldırım HC. Fatigue strength assessment of HFMI-treated butt welds by the effective notch stress method. *Weld World.* 2014; 58:279-288.
 17. Leitner M, Simunek D, Shah SF, Stoschka M. Numerical fatigue assessment of welded and HFMI-treated joints by notch stress/strain and fracture mechanical approaches. *Adv Eng Softw.* 2018;120:96-106.
 18. Zerbst U, Madia M, Vormwald M. Applying fracture mechanics to fatigue strength determination – Some basic considerations. *Int J Fatigue.* 2019;126:188-201.
 19. Nykanen T, Marquis G, Bjork T. A simplified fatigue assessment method for high quality welded cruciform joints. *Int J Fatigue.* 2009;31:79-87.
 20. Mikkola E, Murakami Y, Marquis G. Equivalent crack approach for fatigue life assessment of welded joints. *Eng Fract Mech.* 2015;149:144-155.
 21. Sonsino C. Multiaxial fatigue of welded joints under in-phase and out-of-phase local strains and stresses. *Int J Fatigue.* 1995; 17:55-70.
 22. Susmel L. *Multiaxial notch fatigue.* Cambridge, UK: Woodhead Publishing; 2009.
 23. Radaj D, Vormwald M. *Advanced Methods of Fatigue Assessment.* Berlin, Heidelberg: Springer Berlin Heidelberg; 2013. Epub ahead of print 2013. doi:10.1007/978-3-642-30740-9.
 24. Lazzarin P, Tovo R. A notch intensity factor approach to the stress analysis of welds. *Fatigue Fract Eng Mater Struct.* 1998; 21:1089-1103.
 25. Lazzarin P, Sonsino CM, Zambardi R. A notch stress intensity approach to assess the multiaxial fatigue strength of welded tube-to-flange joints subjected to combined loadings. *Fatigue Fract Eng Mater Struct.* 2004;27:127-140.
 26. Fischer C, Fricke W, Rizzo CM. Experiences and recommendations for numerical analyses of notch stress intensity factor and averaged strain energy density. *Eng Fract Mech.* 2016;165: 98-113.
 27. Fischer C, Fricke W, Rizzo CM. Review of the fatigue strength of welded joints based on the notch stress intensity factor and SED approaches. *Int J Fatigue.* 2016;84:59-66.
 28. Livieri P, Lazzarin P. Fatigue strength of steel and aluminium welded joints based on generalised stress intensity factors and local strain energy values. *Int J Fract.* 2005;133:247-276.
 29. Lazzarin P, Livieri P, Berto F, Zappalorto M. Local strain energy density and fatigue strength of welded joints under uniaxial and multiaxial loading. *Eng Fract Mech.* 2008;75: 1875-1889.
 30. Foti P, Santonocito D, Risitano G, Berto F. Fatigue assessment of cruciform joints: Comparison between Strain Energy Density predictions and current standards and recommendations. *Eng Struct.* 2021;230:111708.
 31. Song W, Liu X, Razavi SMJ. Fatigue assessment of steel load-carrying cruciform welded joints by means of local approaches. *Fatigue Fract Eng Mater Struct.* 2018;41:2598-2613.
 32. Carpinteri A, Spagnoli A, Vantadori S. Multiaxial fatigue life estimation in welded joints using the critical plane approach. *Int J Fatigue.* 2009;31:188-196.
 33. Susmel L. Modified Wöhler curve method, theory of critical distances and Eurocode 3: A novel engineering procedure to predict the lifetime of steel welded joints subjected to both uniaxial and multiaxial fatigue loading. *Int J Fatigue.* 2008;30: 888-907.
 34. Susmel L. The Modified Wöhler Curve Method calibrated by using standard fatigue curves and applied in conjunction with the Theory of Critical Distances to estimate fatigue lifetime of aluminium weldments. *Int J Fatigue.* 2009;31:197-212.
 35. Meneghetti G, Campagnolo A. State-of-the-art review of peak stress method for fatigue strength assessment of welded joints. *Int J Fatigue.* 2020;139:105705.
 36. Williams ML. Stress singularities resulting from various boundary conditions in angular corners of plates in tension. *J Appl Mech.* 1952;19:526-528.
 37. Qian J, Hasebe N. Property of eigenvalues and eigenfunctions for an interface V-notch in antiplane elasticity. *Eng Fract Mech.* 1997;56:729-734.
 38. Gross B, Mendelson A. Plane elastostatic analysis of V-notched plates. *Int J Fract Mech.* 1972;8:267-276.
 39. Lazzarin P, Tovo R. A unified approach to the evaluation of linear elastic stress fields in the neighborhood of cracks and notches. *Int J Fract.* 1996;78:3-19.
 40. Verreman Y, Nie B. Early development of fatigue cracking at manual fillet welds. *Fatigue Fract Eng Mater Struct.* 1996;19: 669-681.
 41. Atzori B, Meneghetti G. Fatigue strength of fillet welded structural steels: finite elements, strain gauges and reality. *Int J Fatigue.* 2001;23:713-721.
 42. Lazzarin P, Lassen T, Livieri P. A notch stress intensity approach applied to fatigue life predictions of welded joints with different local toe geometry. *Fatigue Fract Eng Mater Struct.* 2003;26:49-58.
 43. Nisitani H, Teranishi T. KI of a circumferential crack emanating from an ellipsoidal cavity obtained by the crack tip stress method in FEM. *Eng Fract Mech.* 2004;71:579-585.
 44. Meneghetti G, Lazzarin P. Significance of the elastic peak stress evaluated by FE analyses at the point of singularity of sharp V-notched components. *Fatigue Fract Eng Mater Struct.* 2007;30: 95-106.
 45. Meneghetti G, Guzzella C. The peak stress method to estimate the mode I notch stress intensity factor in welded joints using three-dimensional finite element models. *Eng Fract Mech.* 2014;115:154-171.
 46. Meneghetti G. The use of peak stresses for fatigue strength assessments of welded lap joints and cover plates with toe and root failures. *Eng Fract Mech.* 2012;89:40-51.
 47. Meneghetti G. The peak stress method for fatigue strength assessment of tube-to-flange welded joints under torsion loading. *Weld World.* 2013;57:265-275.
 48. Meneghetti G, Campagnolo A, Avalle M, et al. Rapid evaluation of notch stress intensity factors using the peak stress method: Comparison of commercial finite element codes for a range of mesh patterns. *Fatigue Fract Eng Mater Struct.* 2018; 41(5):1044-1063. doi:10.1111/ffe.12751
 49. Campagnolo A, Meneghetti G. Rapid estimation of notch stress intensity factors in 3D large-scale welded structures using the peak stress method. *MATEC Web Conf.* 2018;165:17004. doi: 10.1051/matecconf/201816517004
 50. Campagnolo A, Roveda I, Meneghetti G. The Peak Stress Method combined with 3D finite element models to assess the

- fatigue strength of complex welded structures. *Procedia Struct Integr.* 2019;19:617-626.
51. Meneghetti G, Campagnolo A, Rigon D. Multiaxial fatigue strength assessment of welded joints using the Peak Stress Method—part II: Application to structural steel joints. *Int J Fatigue.* 2017;101:343-362.
 52. Lepore M, Solberg K, Berto F. A comparison between numerical and approximate methods for rapid calculation of NSIFs. *Theor Appl Fract Mech.* 2019;101:67-79.
 53. Lazzarin P, Berto F, Zappalorto M. Rapid calculations of notch stress intensity factors based on averaged strain energy density from coarse meshes: Theoretical bases and applications. *Int J Fatigue.* 2010;32:1559-1567.
 54. Zappalorto M, Carraro PA. An efficient energy-based approach for the numerical assessment of mode I NSIFs in isotropic and orthotropic notched plates. *Theor Appl Fract Mech.* 2020;108:102612.
 55. Zappalorto M, Pontefisso A, Carraro PA. On the use of elemental quantities to compute NSIFs at pointed V-notches with non-regular coarse meshes. *Theor Appl Fract Mech.* 2021;116:103083.
 56. Foti P, Ayatollahi MR, Berto F. Rapid strain energy density evaluation for V-notches under mode I loading conditions. *Eng Fail Anal.* 2020;110:104361.
 57. Campagnolo A, Zuin S, Meneghetti G. Averaged strain energy density estimated rapidly from nodal displacements by coarse FE analyses: cracks under mixed mode loadings. *Fatigue Fract Eng Mater Struct.* 2020;43:1658-1685.
 58. Meneghetti G, Campagnolo A, Berto F, Atzori B. Averaged strain energy density evaluated rapidly from the singular peak stresses by FEM: cracked components under mixed-mode (I + II) loading. *Theor Appl Fract Mech.* 2015;79:113-124.
 59. Campagnolo A, Meneghetti G, Berto F. Rapid finite element evaluation of the averaged strain energy density of mixed-mode (I + II) crack tip fields including the T-stress contribution. *Fatigue Fract Eng Mater Struct.* 2016;39:982-998.
 60. Meneghetti G, Campagnolo A, Berto F. Averaged strain energy density estimated rapidly from the singular peak stresses by FEM: cracked bars under mixed-mode (I+III) loading. *Eng Fract Mech.* 2016;167:20-33.
 61. Campagnolo A, Vormwald M, Shams E, Meneghetti G. Multiaxial fatigue assessment of tube-tube steel joints with weld ends using the peak stress method. *Int J Fatigue.* 2020;135:105495.
 62. Meneghetti G, Lazzarin P. The Peak Stress Method for Fatigue Strength Assessment of welded joints with weld toe or weld root failures. *Weld World.* 2011;55:22-29.
 63. Meneghetti G, Campagnolo A, Rigon D. Multiaxial fatigue strength assessment of welded joints using the Peak Stress Method—part I: approach and application to aluminium joints. *Int J Fatigue.* 2017;101:328-342.
 64. Meneghetti G, Campagnolo A. Fatigue of welded components. In: *Comprehensive Structural Integrity*. Elsevier; 2021. Epub ahead of print 2021. doi:10.1016/B978-0-12-822944-6.00003-7
 65. Radaj D. State-of-the-art review on extended stress intensity factor concepts. *Fatigue Fract Eng Mater Struct.* 2014;37:1-28.
 66. Radaj D. State-of-the-art review on the local strain energy density concept and its relation to the J -integral and peak stress method. *Fatigue Fract Eng Mater Struct.* 2015;38:2-28.
 67. Berto F, Lazzarin P. Recent developments in brittle and quasi-brittle failure assessment of engineering materials by means of local approaches. *Mater Sci Eng R Reports.* 2014;75:1-48.
 68. Campagnolo A, Ferro P, Romanin L, Meneghetti G. Residual notch stress intensity factors in welded joints evaluated by 3D numerical simulations of arc welding processes. *Materials (Basel).* 2021;14(4):812. doi:10.3390/ma14040812
 69. Zienkiewicz OC, Taylor RL, Zhu JZ. *The Finite Element Method: Its Basis and Fundamentals*. Elsevier; 2013. Epub ahead of print 2013. doi:10.1016/C2009-0-24909-9
 70. Bathe KJ. *Finite Element Procedures*. Pearson College Div; 1995.

How to cite this article: Meneghetti G, Campagnolo A, Visentin A, et al. Rapid evaluation of notch stress intensity factors using the peak stress method with 3D tetrahedral finite element models: Comparison of commercial codes. *Fatigue Fract Eng Mater Struct.* 2022;1-30.
doi:10.1111/ffe.13645

APPENDIX A

DETAILS OF MESH GENERATION SETTINGS

Details relevant to element type and settings to generate a free 3D FE mesh are reported in the following for each FE code:

- Ansys® Mechanical APDL

Element type: Solid → Tet 4-node (SOLID 285) or Tet 10-node (SOLID 187).

Element options: not applicable.

Element size: Size Cntrls → Manual Size → Global → Size = d .

Mesh generation: Mesh → Volumes → Free

- Ansys® Mechanical

Element type: Tet4 (SOLID 185) or Tet10 (SOLID 187).

Element options: not applicable.

Element size: Mesh → Insert → Sizing → Type = Element Size → Element Size = d .

Mesh generation: Mesh → Insert → Method → Method = Tetrahedrons → Element Order = Linear (for Tet4) or Quadratic (for Tet10); Mesh → Sizing → Use Adaptive Sizing = No → Mesh Defeaturing = No; Mesh → Generate Mesh

- Dassault Systèmes® Abaqus

Element type: Tet C3D4 or C3D10.

Element options: not applicable.

Element size: Global Seeds → Sizing Cntrls → Approximate global size = d .

Mesh generation: Mesh Cntrls → Tet → Free → Use default algorithm → “Use mapped tri meshing on bounding faces where appropriate” MUST BE INACTIVE; Mesh Part Instance → Ok

- Lusas®

Element type: 3D isoparametric tetrahedra solid continuum element with higher order models capable of modeling curved boundaries (TH4).

Element options: 4 (TH4) or 10 (TH10) nodes.

Element size: Mesh → Volume Mesh → Irregular mesh → Element size = d .

Mesh generation: Mesh → Volume Mesh

- Dassault Systèmes® Solidworks

Element type: First-order tetrahedral (Draft quality) or Second-order tetrahedral (High quality).

Element options: not applicable.

Element Size and Mesh generation: Mesh → Create Mesh → Definition → Mesh Parameters: Blended

curvature-based mesh; Maximum element size = Minimum element size = d ; Mesh Quality → Specify: Draft or High → OK

- Altair® Hypermesh/LS-Dyna/Hyperview

Element type: Tetrahedral 4 nodes Elform 10, tetrahedral 10 nodes Elform 17 (*LS-Dyna*).

Element options: not applicable.

Element size: 2D → Automesh → Surfs → Size and bias → Element size = d (*Hypermesh*).

Mesh generation: 2D → Automesh → Surfs → Size and bias → Mesh type → trias; mesh → 3D → Tetramesh → Tetrahedral mesh → Fixed trias/quads to tetrahedral mesh; mesh (*Hypermesh*)

- Altair® Hypermesh/Optistruct/Hyperview

Element type: CTETRAHEDRAL (*Hypermesh*).

Element options: not applicable, default tetrahedral formulation (*Optistruct*).

Element size: 3D → Tetramesh → Element size = d (*Hypermesh*).

Mesh generation: 3D → Tetramesh → Volume tetrahedral → 3D type: tetras; element order: first/second (*Hypermesh*).